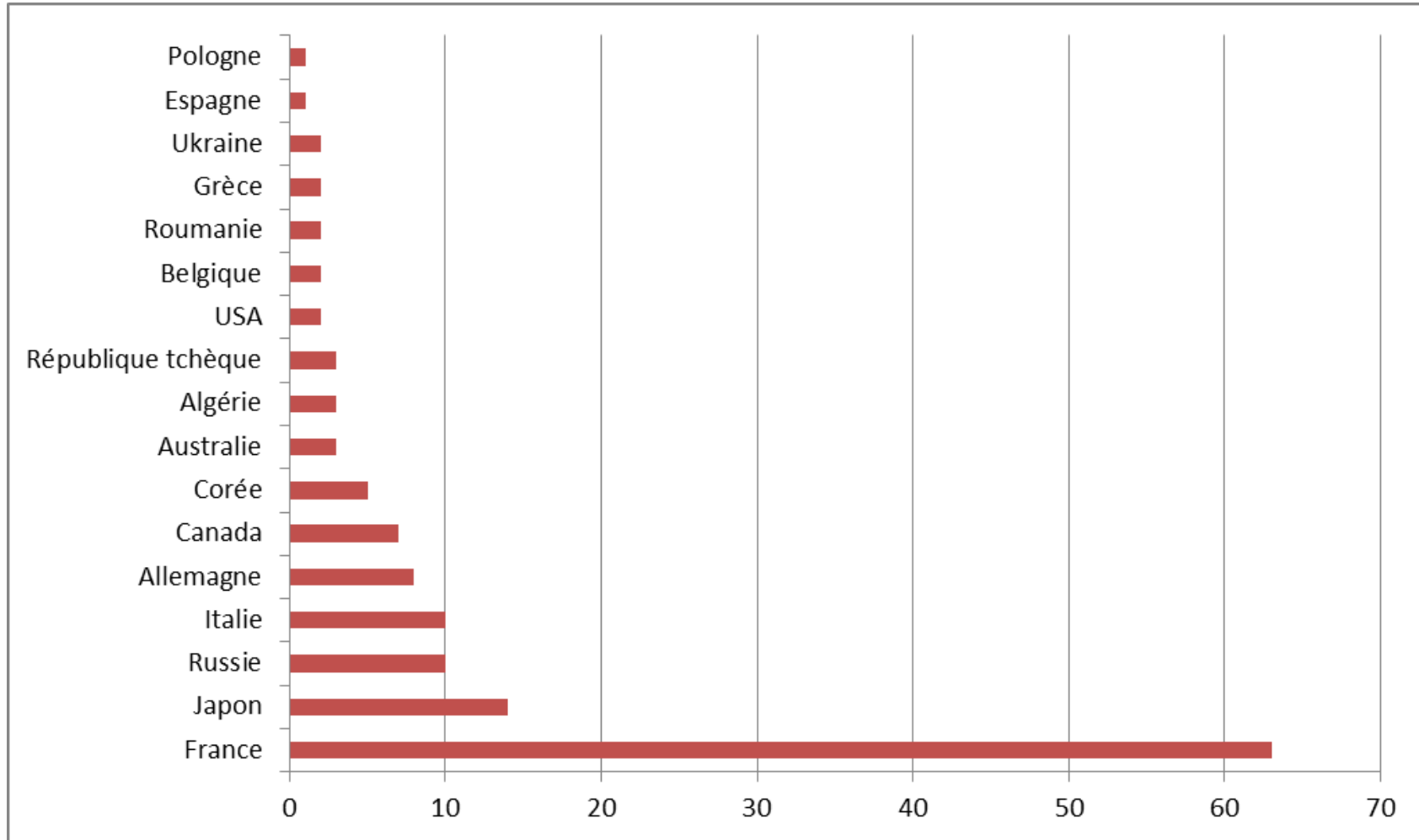


22-27 June 2014, TOULOUSE

- **142 participants**
- **140 présentations**
- **Equilibre entre plasmas thermiques et plasmas non thermiques**
- **8 conférences invitées plénières**
- **8 conférences invitées thématiques**
- **58 oraux + 82 posters. Pas de sessions parallèles**

Répartition des participants



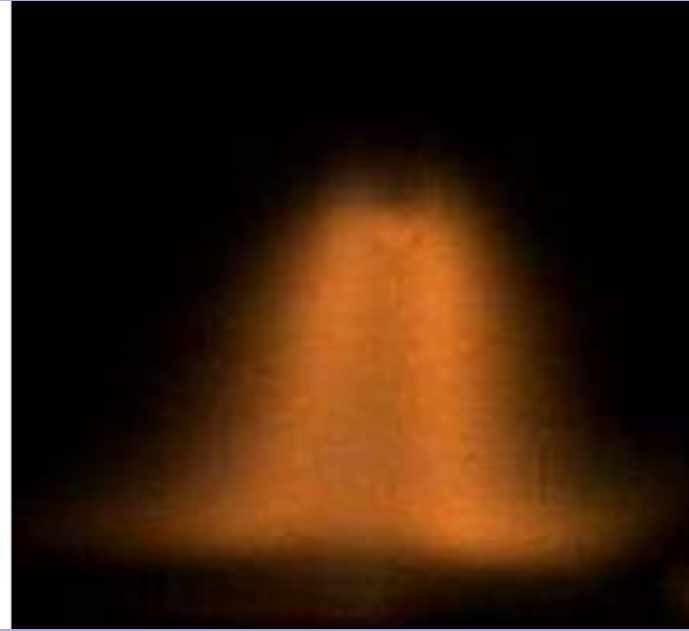
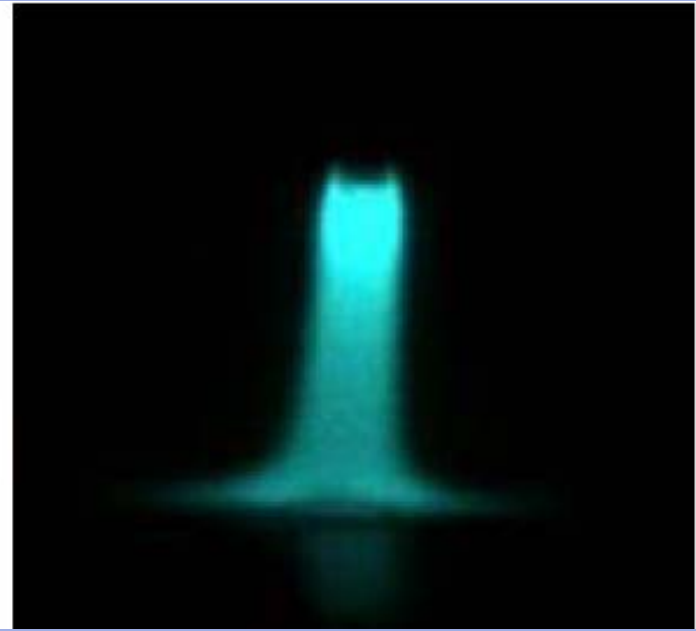
Répartition des thématiques



- Depôt et traitement surface
- Plasmas hors équilibre
- Combustion et Aeronautique
- Environnement et Médecine
- Torches à plasma
- Projection plasma
- Arcs et plasmas thermiques
- Métallurgie
- Synthèse de poudres et nanomatériaux

Métallurgie et interaction arcs-matériaux

1 conférence plénière + 1 conférence invitée



Fe

Ar

The Critical Role of Plasma–Surface Interactions in Thermal Plasma Processes

Tony Murphy

HTPP 2014, Toulouse, 24 June 2014

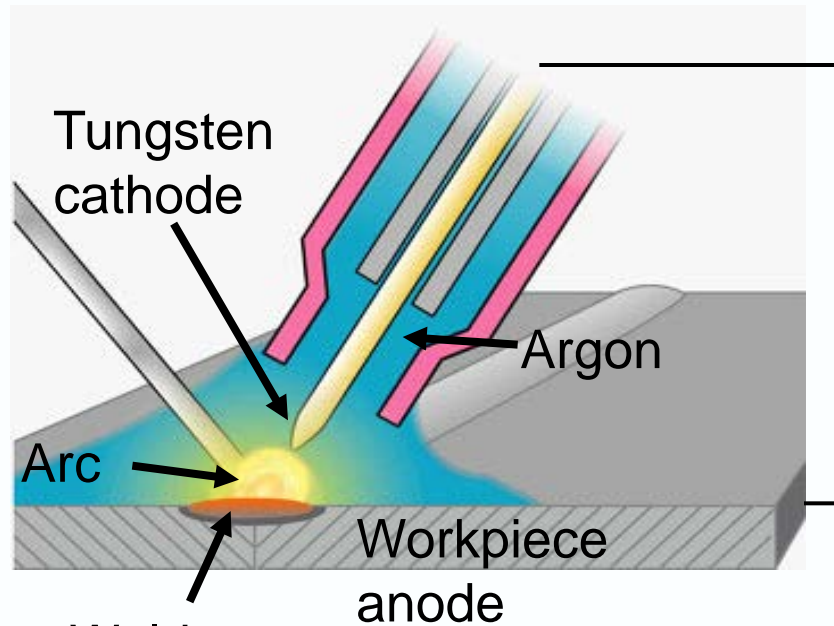
MATERIALS SCIENCE AND ENGINEERING

www.csiro.au



Gas Metal Arc Welding (GMAW) and Gas Tungsten Arc Welding (GTAW)

GTAW (TIG welding)

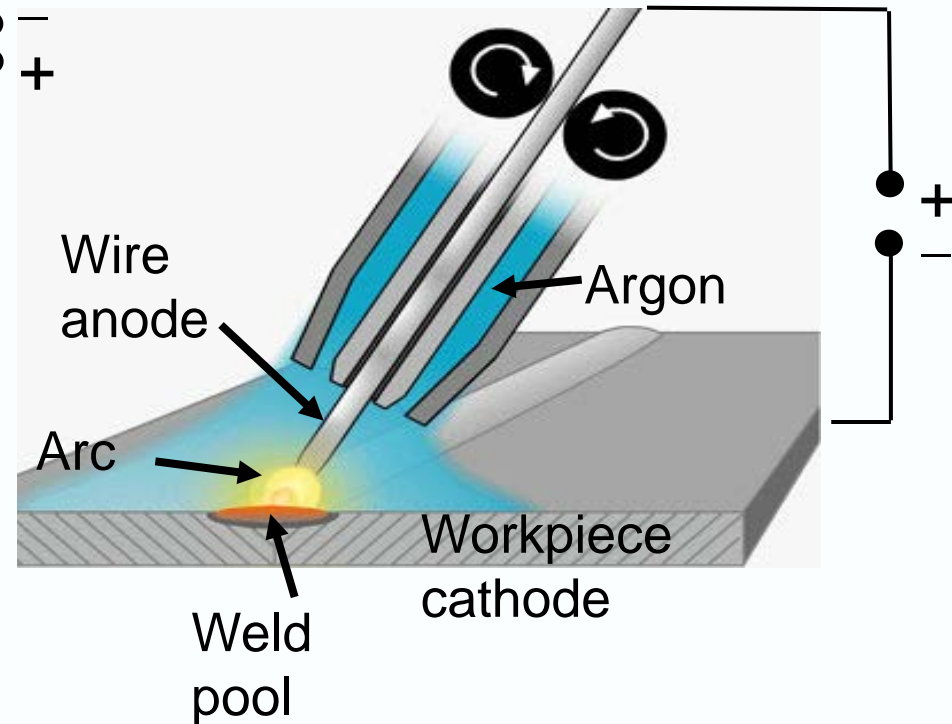


Current ~ 200 A

Power ~ 5 kW

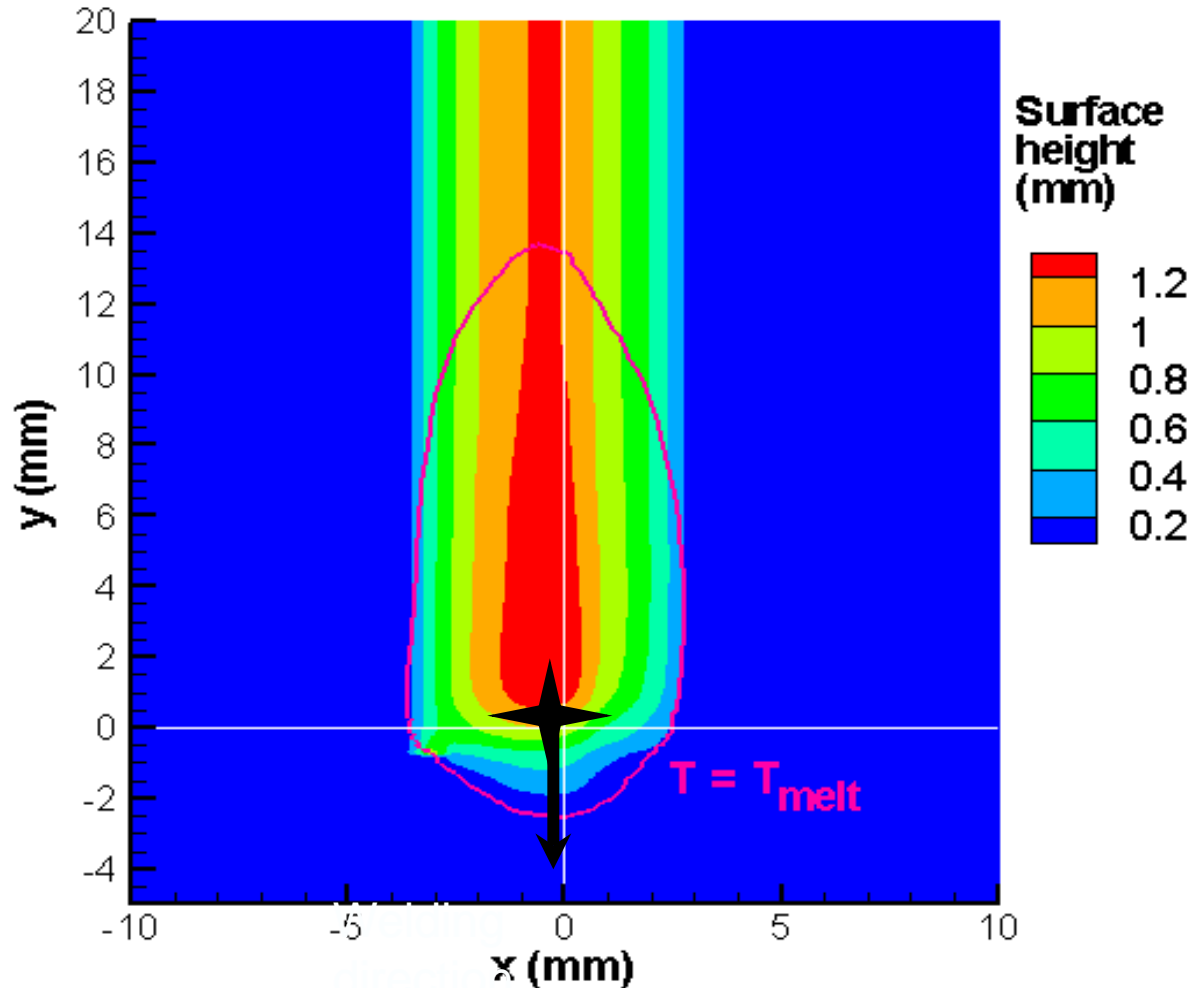
Power density ~ 50 MW m⁻²

GMAW (MIG/MAG welding)



Addition of Droplets to the Weld Pool in GMAW Raises the Surface Height

$I = 95 \text{ A}$, $V_W = -0.9 \text{ m/min}$, $V_{\text{feed}} = 4.3 \text{ m/min}$, $f_{\text{drop}} = 93 \text{ Hz}$, AA 5754

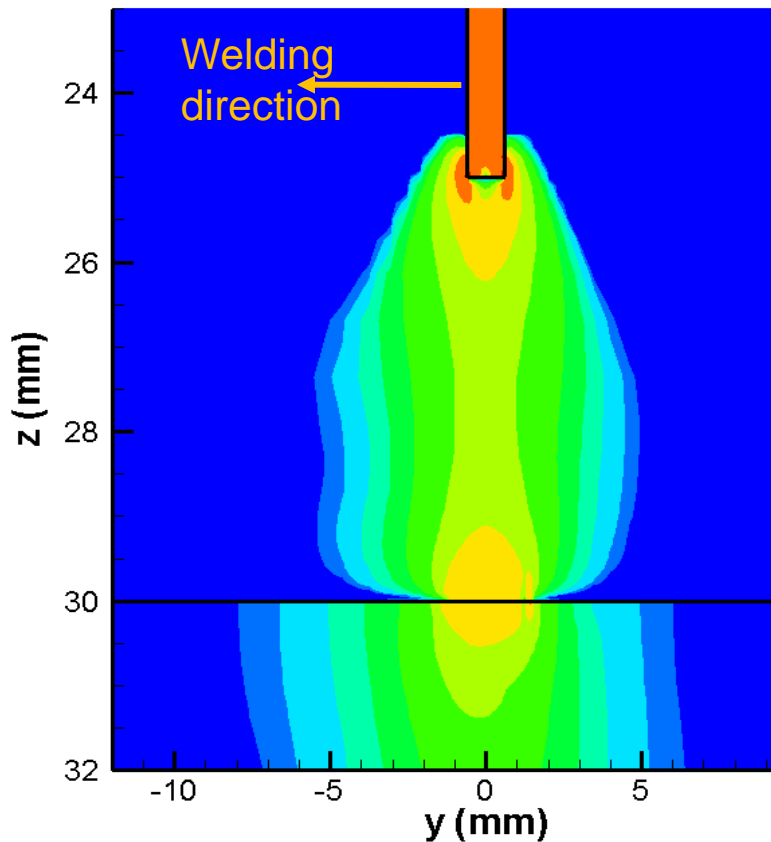


Height of weld pool surface (mm)

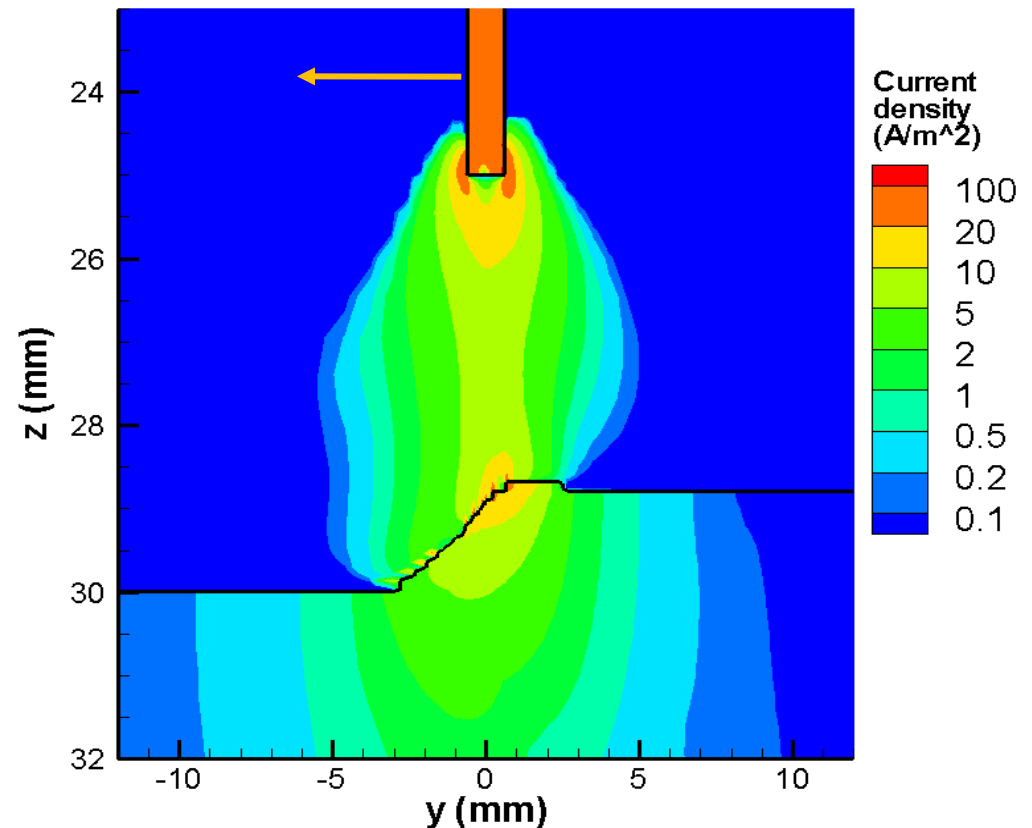
Current Density at Workpiece Strongly Affected by Deformation of Weld Pool Surface

95 A arc, 15 mm/s welding speed, Al alloy AA 5754 workpiece

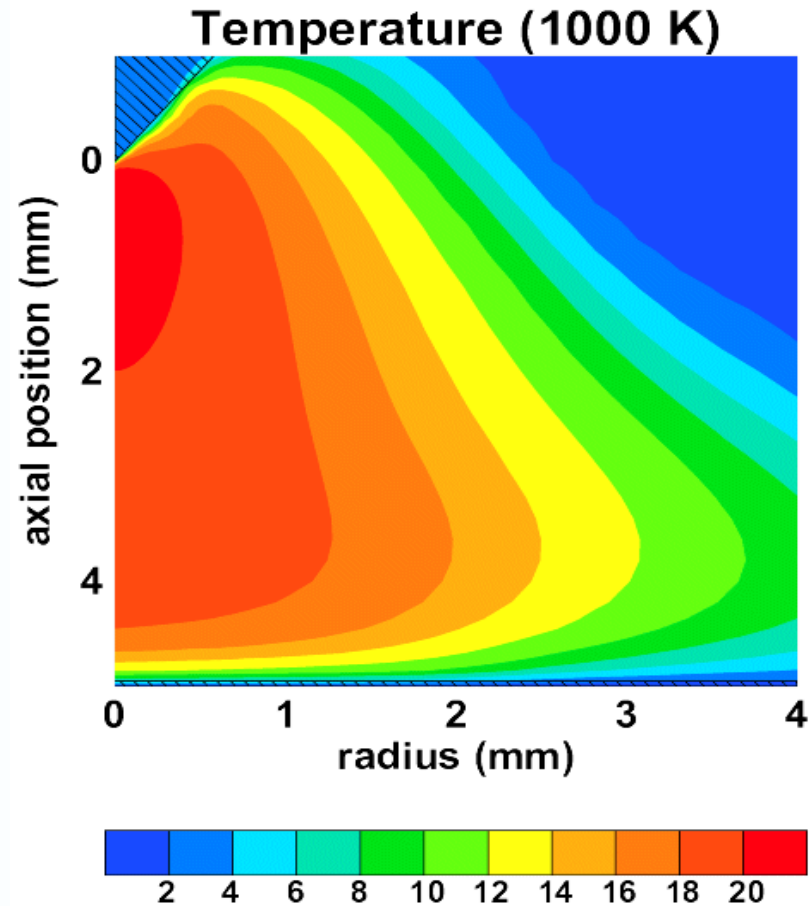
Flat workpiece
(deformation neglected)



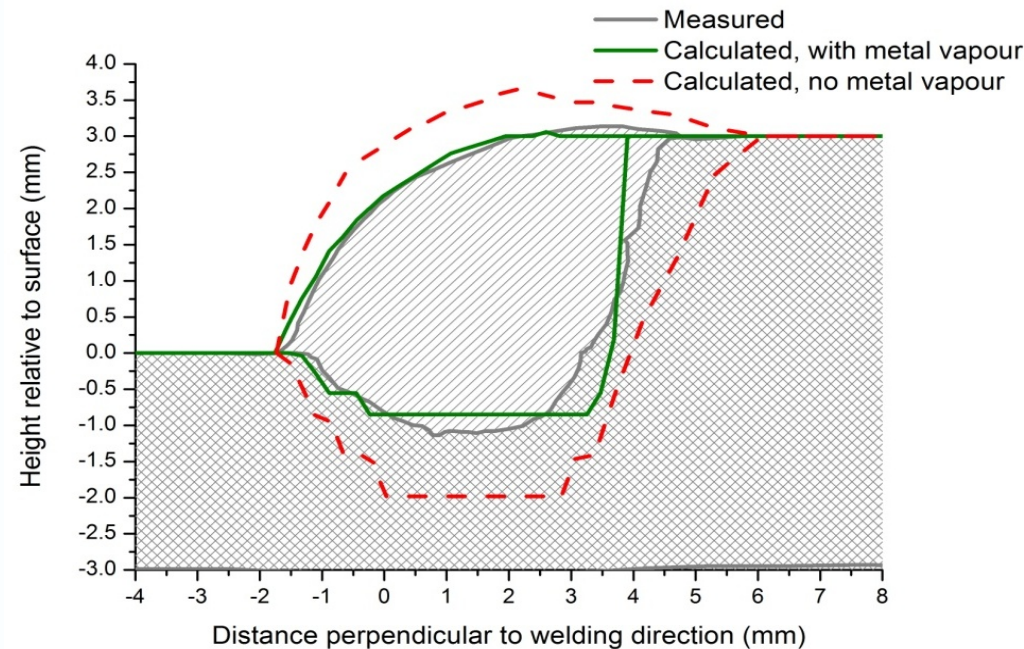
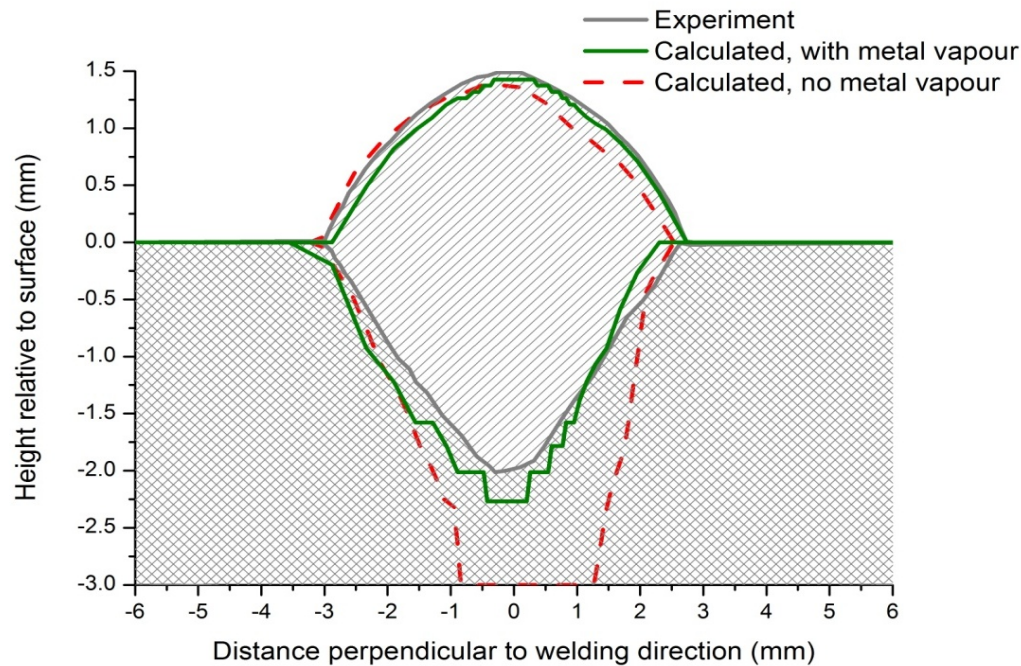
Deformation taken into account



BUT: Two-way interactions are the main reason that it is important to study the thermal plasma



Two-way interactions (metal vapour, weld surface deformation, etc) require the arc plasma to be included in the model



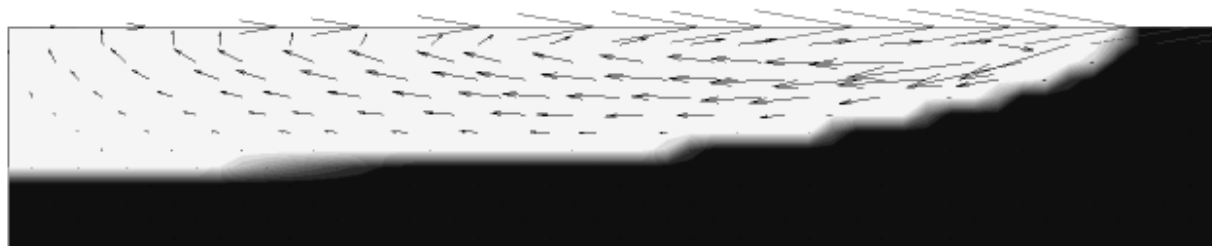
Interaction arc-bain métallique

2 papiers sur modèle et un sur l'expérience.

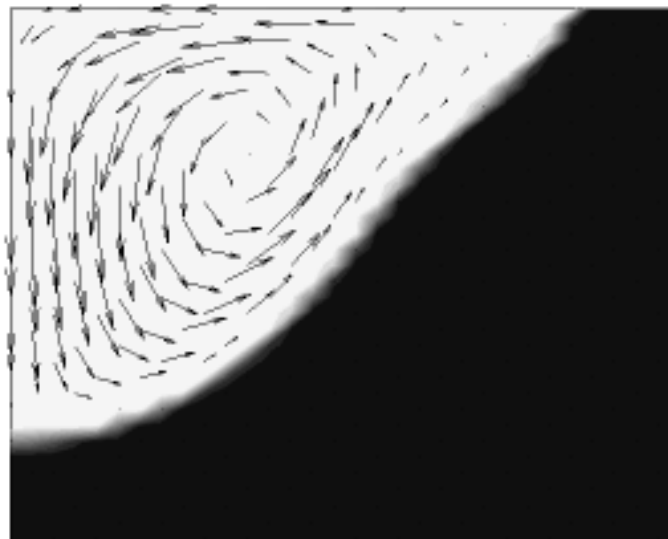
Toropchin et al:
Greifswald

Comparison of the results for the direction of liquid metal movement and weld pool profile of low-alloy steel with Marangoni force addition (a) and without it (b)

(a)

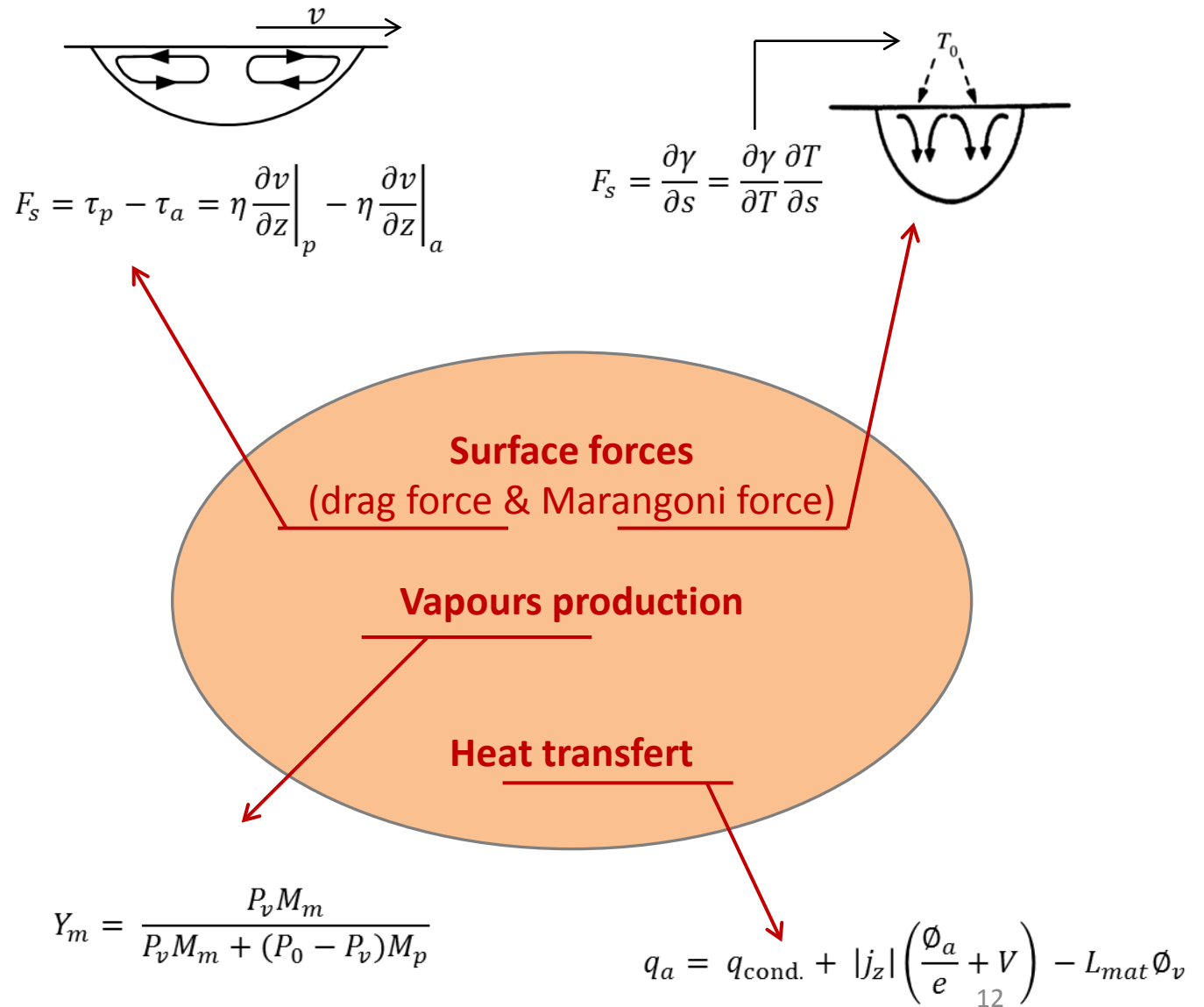


(b)

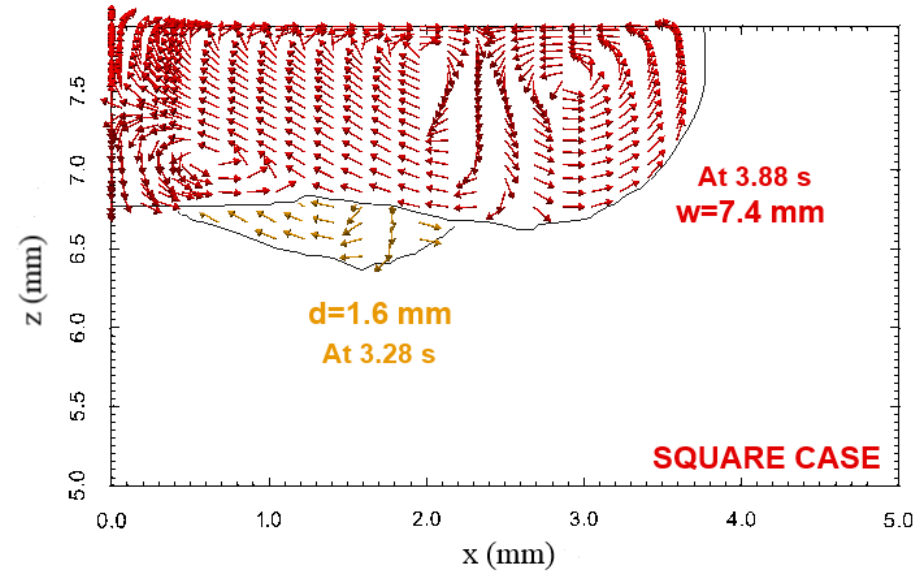
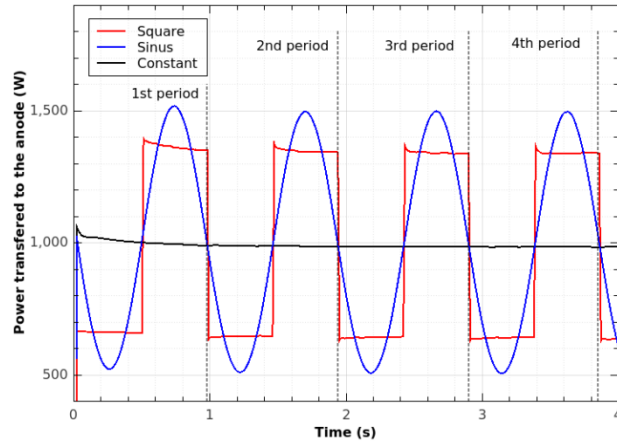


Interaction arc-bain métallique

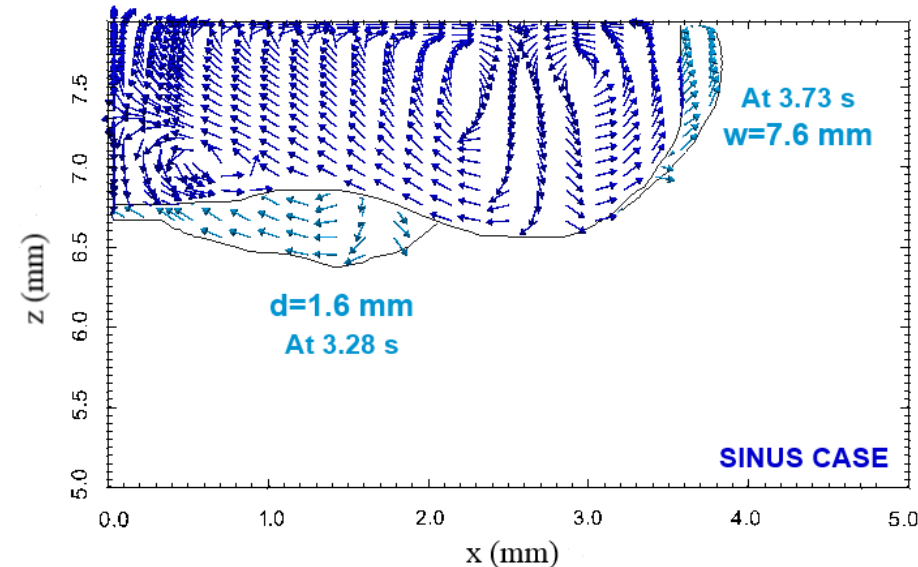
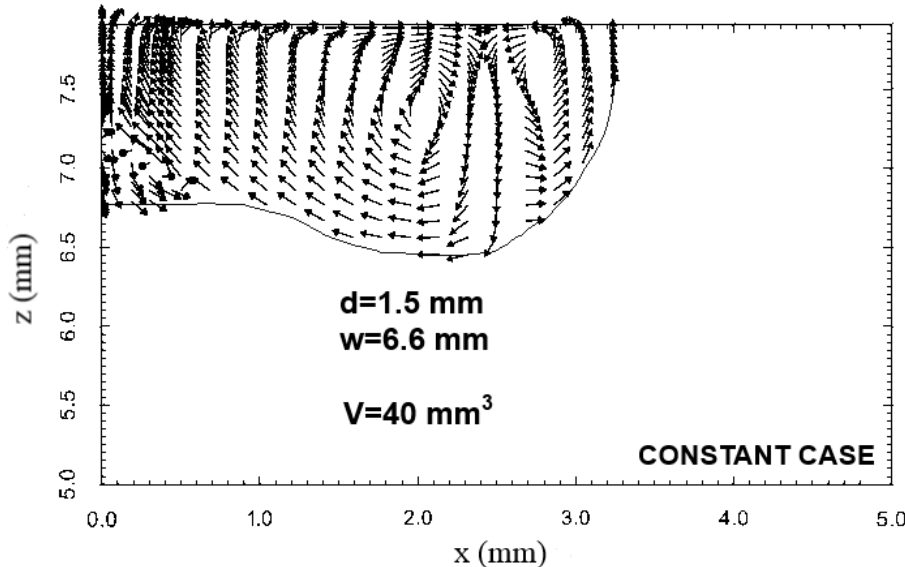
Mougenot et al: LAPLACE
3D model



Interaction arc-bain métallique



Compared to constant case, the square and sinus cases have higher weld dimensions



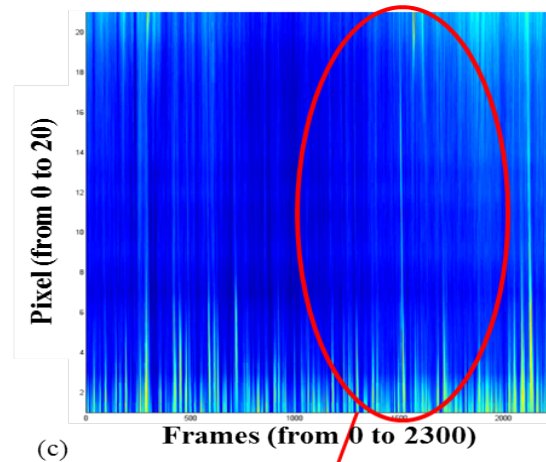
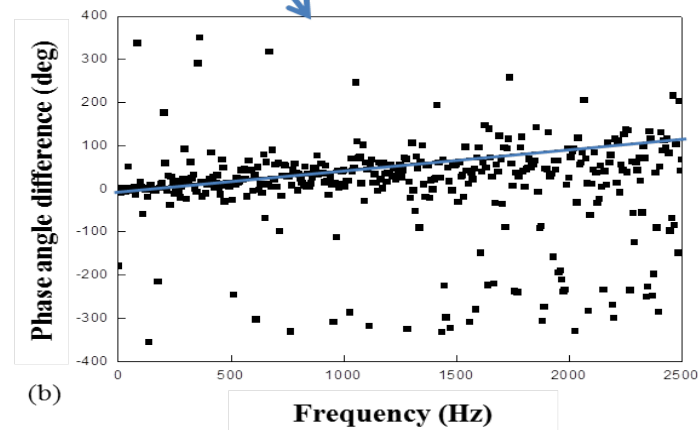
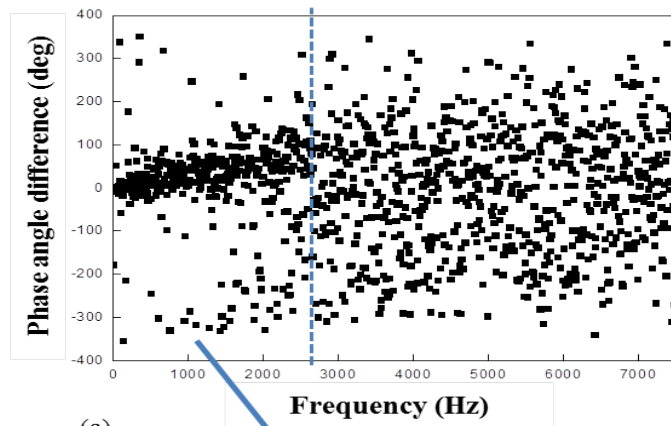
Interaction arc-bain métallique

Stadler et al: LAPLACE. Mesure de flux à la surface d'un bain métallique.

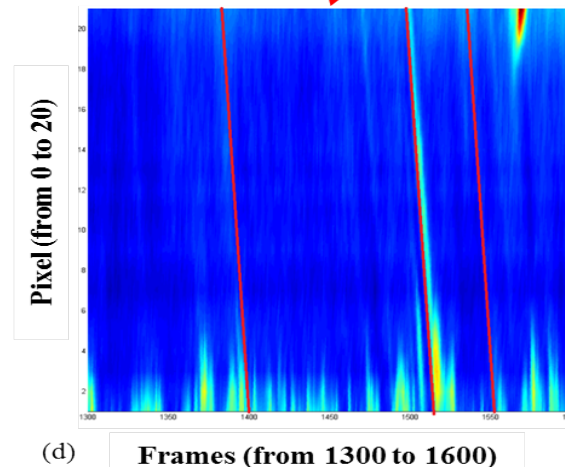
Method 1: Phase angle difference for velocity estimation

Method 2: Bright pixel tracking for velocity estimation

Validation avec goutte d'eau. Application arc transféré He.



0.74 m/s



0.72 m/S

Arc piloté par un champ magnétique alternatif

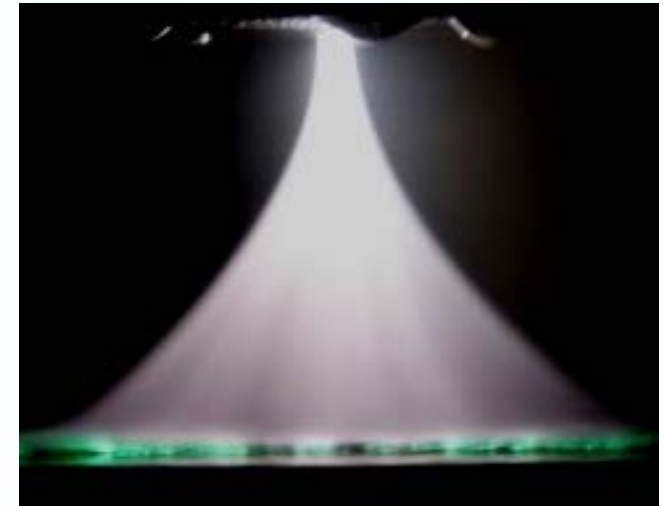
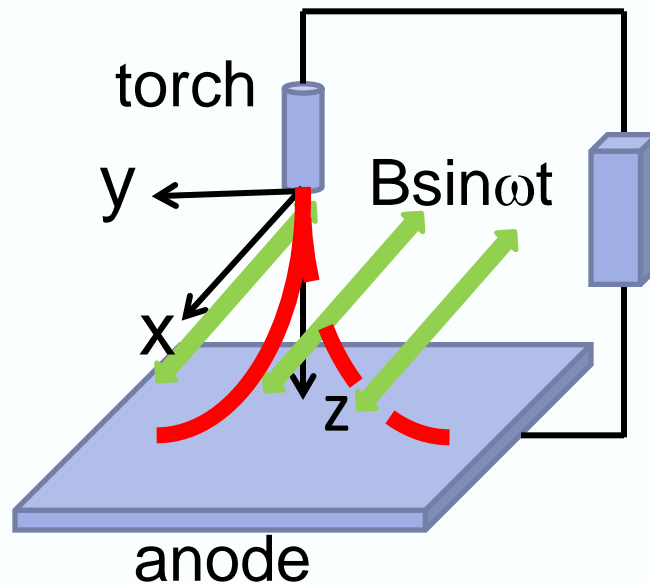
Takeda et al

Schematic illustration of magnetically driven arc



$B=0$

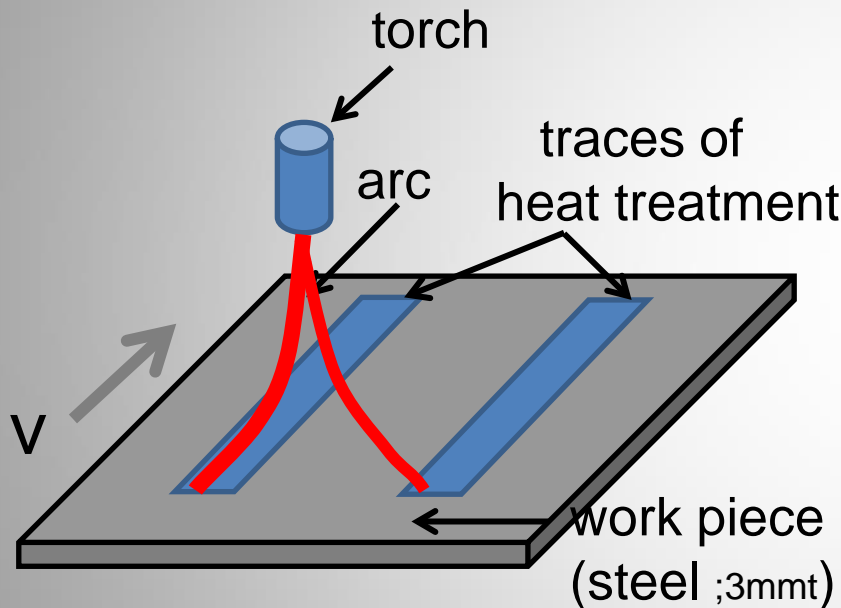
Conventional arc



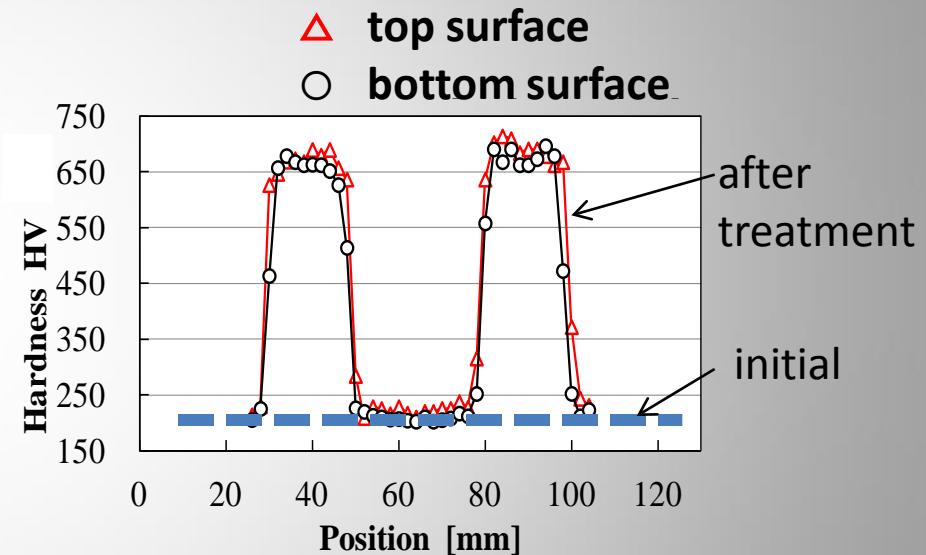
$B=B_0 \sin\omega t$

Magnetically driven arc (MDA)

Example of the application (Heat-treatment of steel)

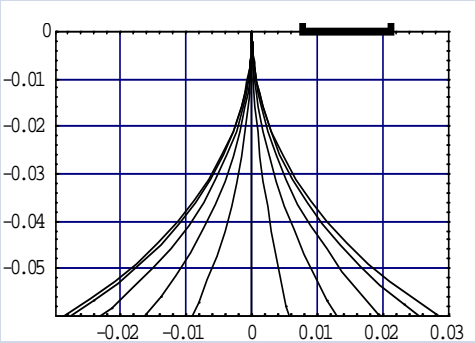
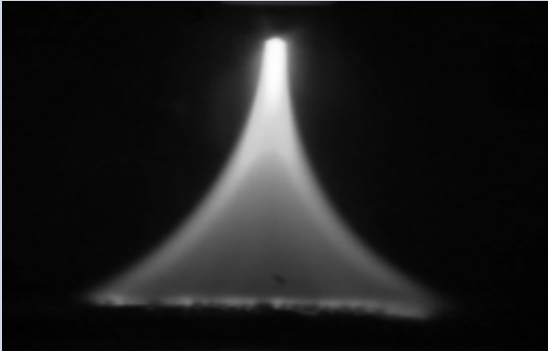
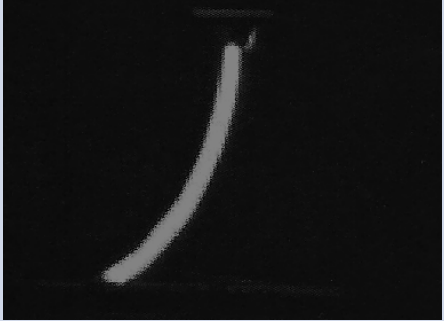
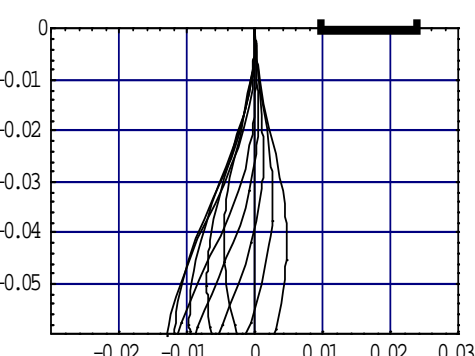

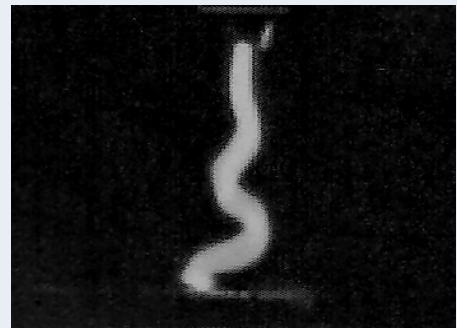


Schematic arrangement for hardening of steel plate using MDA with rectangular form of the magnetic field



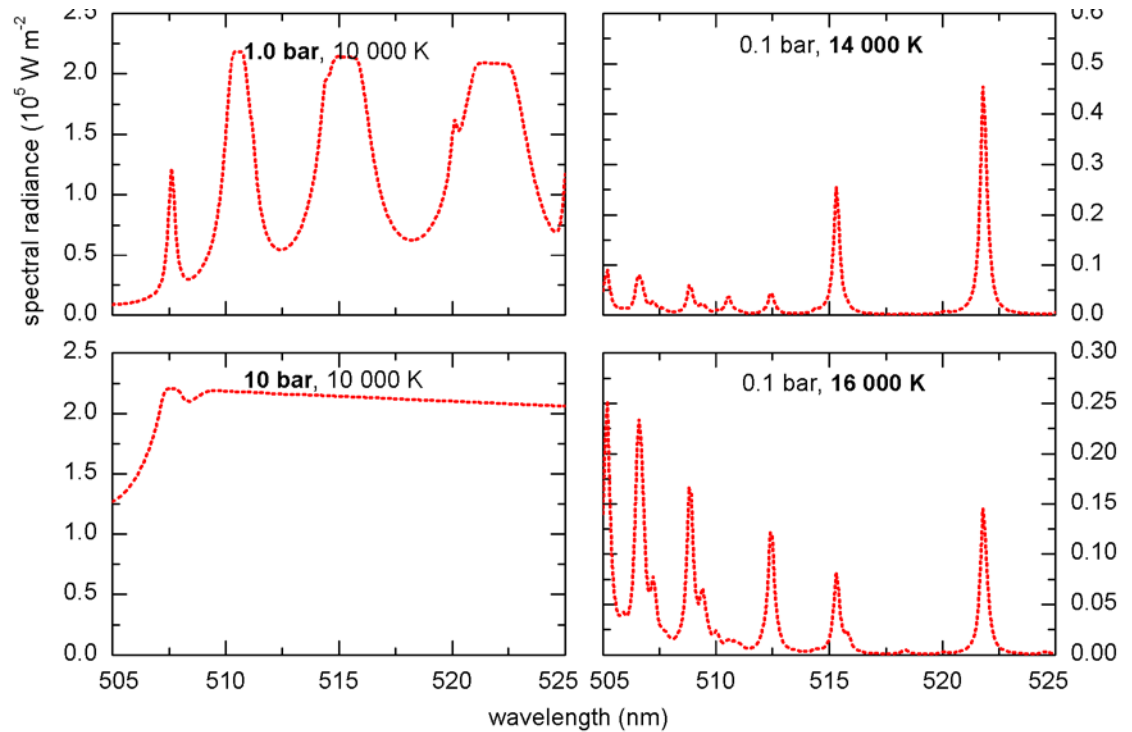
Change of the hardness:
Along two lines of traces, hardness increased about more than 3 times after MDA treatment.

Comparison of Theory with Experiment (Variation of arc profiles with frequency)

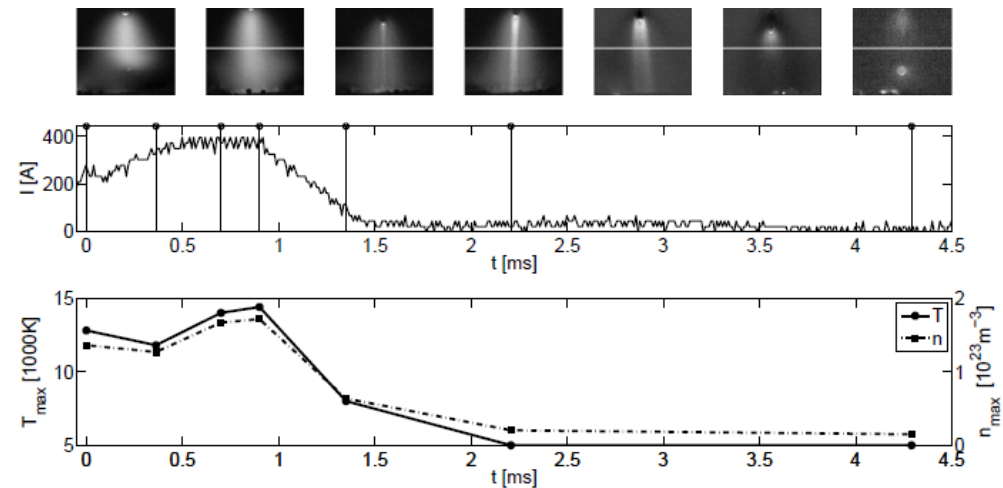
| f (Hz) | Theoretical (for half cycle) | Experimental (exposure: 1/10 sec) | Experimental (exposure: 1/4000 sec) |
|-----------|---|---|--|
| 50 |  <p>Theoretical arc profile for 50 Hz. The graph shows a smooth, symmetric bell-shaped curve centered at 0 on the x-axis. The y-axis ranges from 0 to -0.05, and the x-axis ranges from -0.02 to 0.03. A small horizontal bar is visible at the top right of the plot area.</p> |  <p>Experimental arc profile for 50 Hz with a 1/10 sec exposure. The image shows a smooth, symmetric, bell-shaped arc profile, matching the theoretical prediction.</p> |  <p>Experimental arc profile for 50 Hz with a 1/4000 sec exposure. The image shows a smooth, symmetric, bell-shaped arc profile, matching the theoretical prediction.</p> |
| 1000 |  <p>Theoretical arc profile for 1000 Hz. The graph shows a smooth, symmetric bell-shaped curve centered at 0 on the x-axis. The y-axis ranges from 0 to -0.05, and the x-axis ranges from -0.02 to 0.03. A small horizontal bar is visible at the top right of the plot area.</p> |  <p>Experimental arc profile for 1000 Hz with a 1/10 sec exposure. The image shows a smooth, symmetric, bell-shaped arc profile, matching the theoretical prediction.</p> |  <p>Experimental arc profile for 1000 Hz with a 1/4000 sec exposure. The image shows a smooth, symmetric, bell-shaped arc profile, matching the theoretical prediction.</p> |

Diagnosics dans les arcs

1) Uhrlandt et al (Greifswald).
Arc stabilisé de qqs kA pour étudier
ablation de matériaux.
Spectroscopie d'émission avec raies
de cuivre et prise en compte de l'auto-
absorption des raies



2) Kühn-Kauffeldt et Schein (Munich).
Diffusion Thomson résolue en temps,
sur dispositif de soudage.

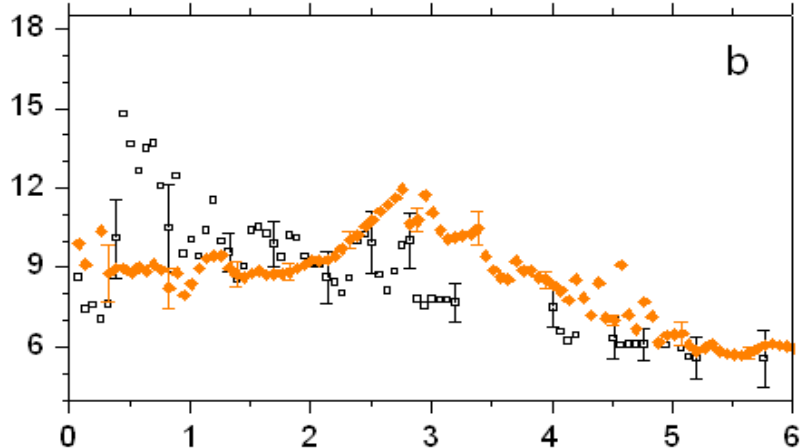
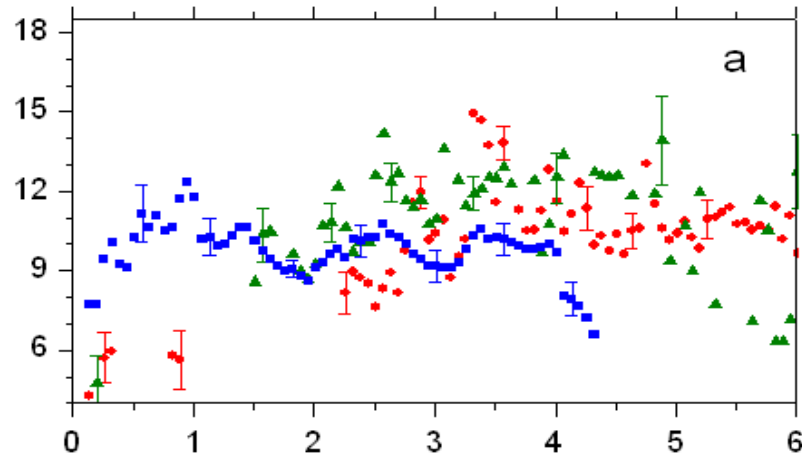
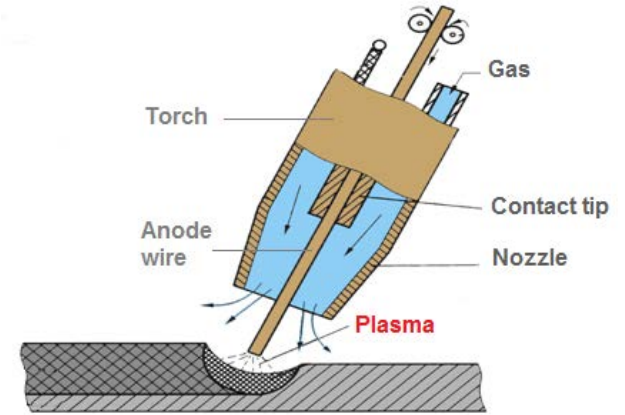


Diagnostics dans les arcs

Etude MIG-MAG: Gremi (Bourges) + Laplace: spectroscopie

→ MIG: Ar, He

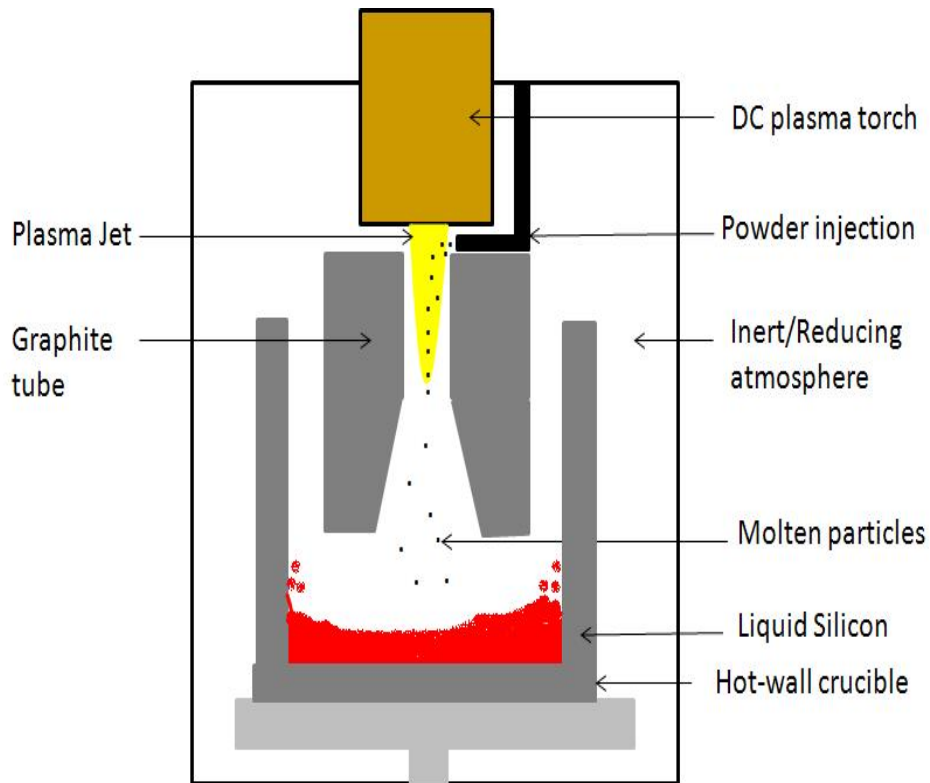
→ MAG: CO₂, O₂, N₂, H₂



- CO₂ ↗:
 - Temperature increase.
 - Maximum away from axis.
- N₂ ↗:
 - Temperature increase.
 - More homogeneous temperature.
- CO₂ ↗:
 - Increase of iron content
- N₂ ↗:
 - Increase of iron content

Purification du silicium

SILIMELT + Limoges: Si cristallin; pureté requise pour panneaux Solaires: 6N = 99,9999%



- Validation of plasma purification of silicon waste for oxide and carbon impurities
- However, silicon purity not high enough for solar-grade silicon because of metallic impurities

→ Combining with acid leaching or directional solidification for metallic impurities removal

Importance de la tuyère en graphite

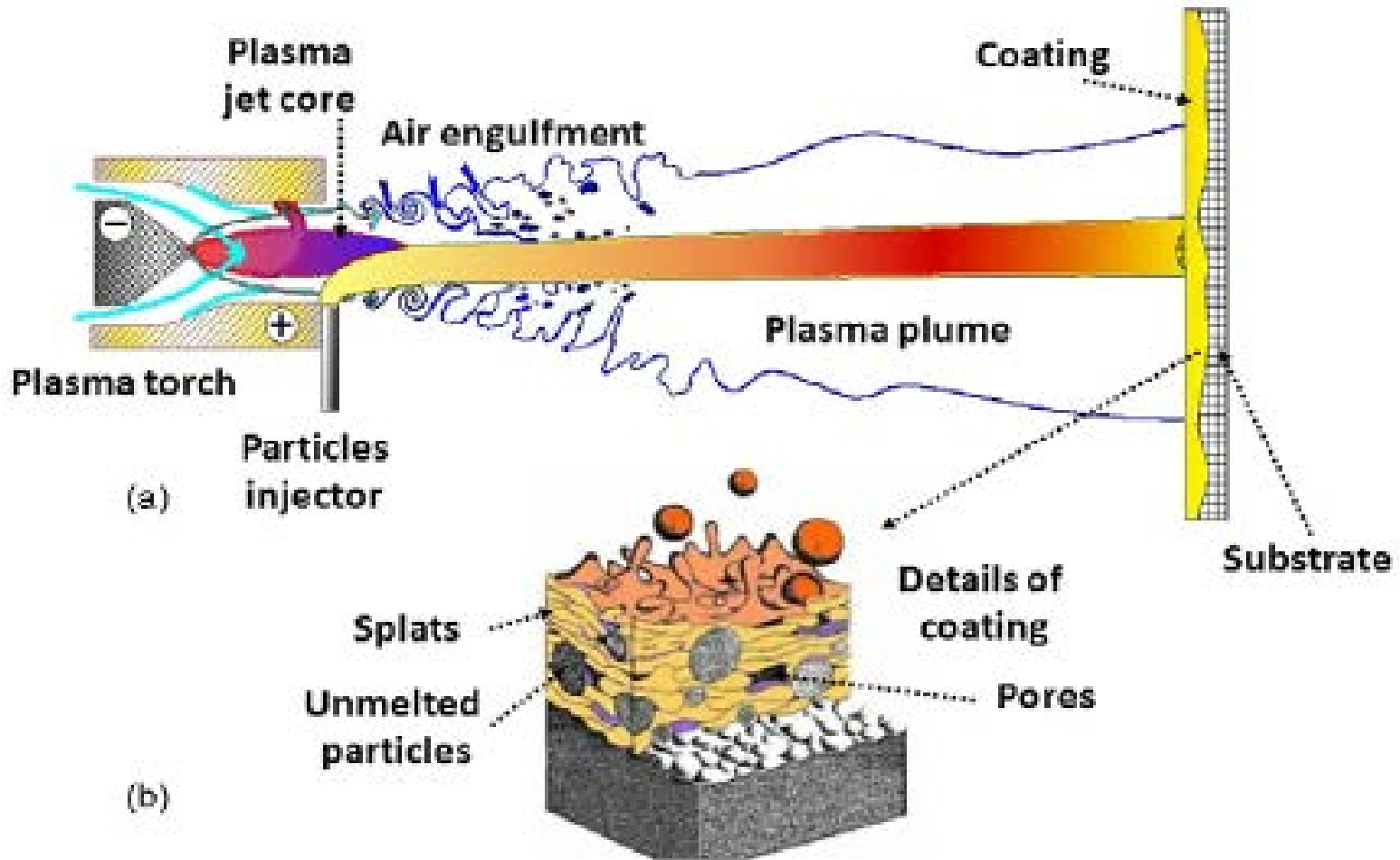
Projection plasma

**1 conférence plénière (Mostaghimi): Towards a complete model of plasma spray process
+ 1 conférence invitée (Fauchais et al):**

Are the Current Plasma Spray Torches Adapted to Suspension Plasma Spraying?

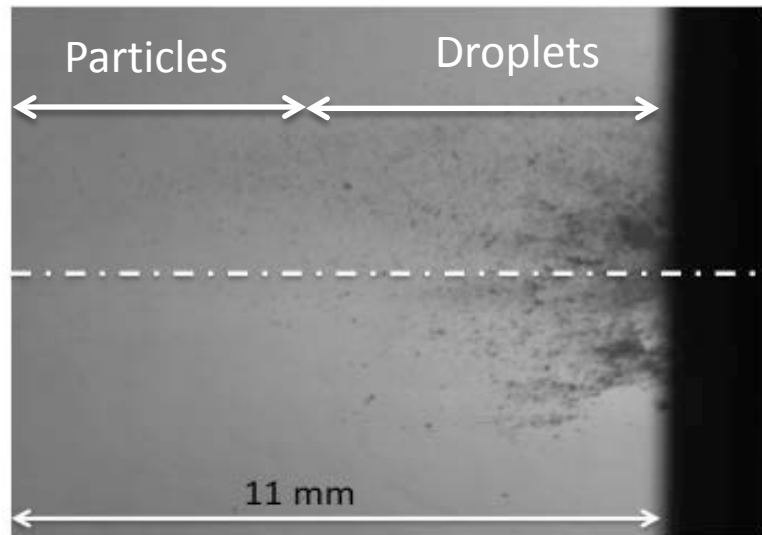
Projection plasma

Are the Current Plasma Spray Torches Adapted to Suspension Plasma Spraying?



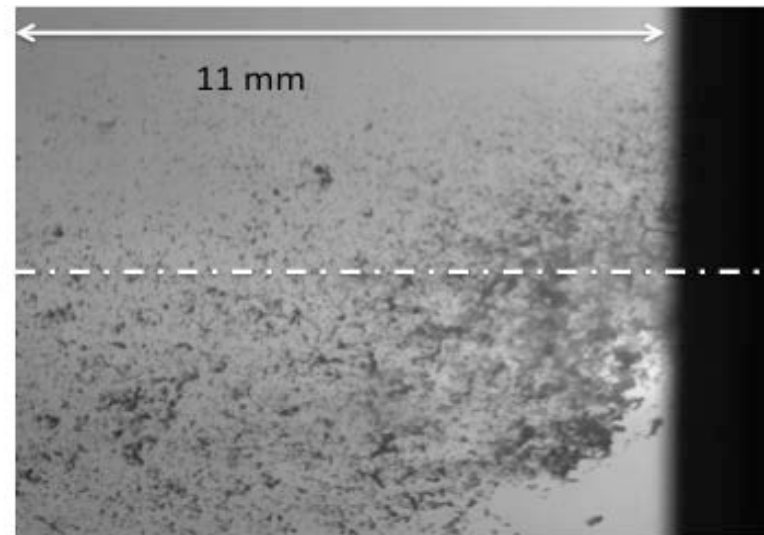
Projection conventionnelle

Plasma liquid interaction: fragmentation and plasma cooling



Pure ethanol

$We = 563$: catastrophic
Rapidly no more droplets
> few μm => no acceleration



Pure water

$We = 170$: stripping

Ar-He
(40-20 L/min)
 $h=14$ MJ/kg

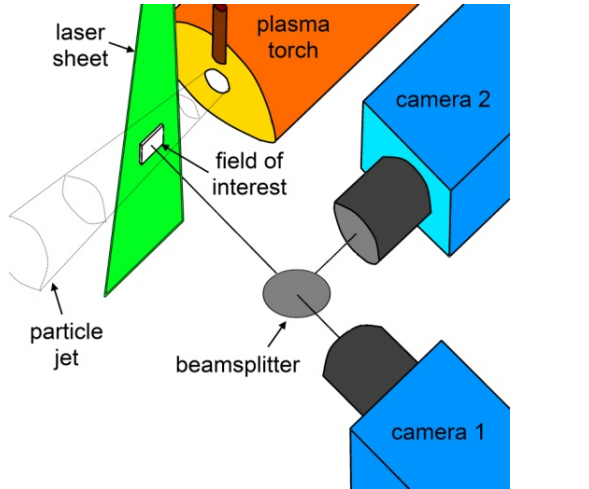
Conclusions

- Mechanisms related to **suspension plasma spraying** **more complex** than those involved in conventional spraying
 - Devices used for **liquid injection** **have to be optimized**
 - control of drop sizes and velocities (narrow distributions)
- Use particles which do not tend agglomerating, as those obtained by chemical routes
 - **Higher power plasma torches** and with low arc voltage fluctuations => **adaptation of plasma torches or specific ones.**
 - **Standards** must be defined for
 - ✓ The plasma spray process
 - ✓ The suspension preparation

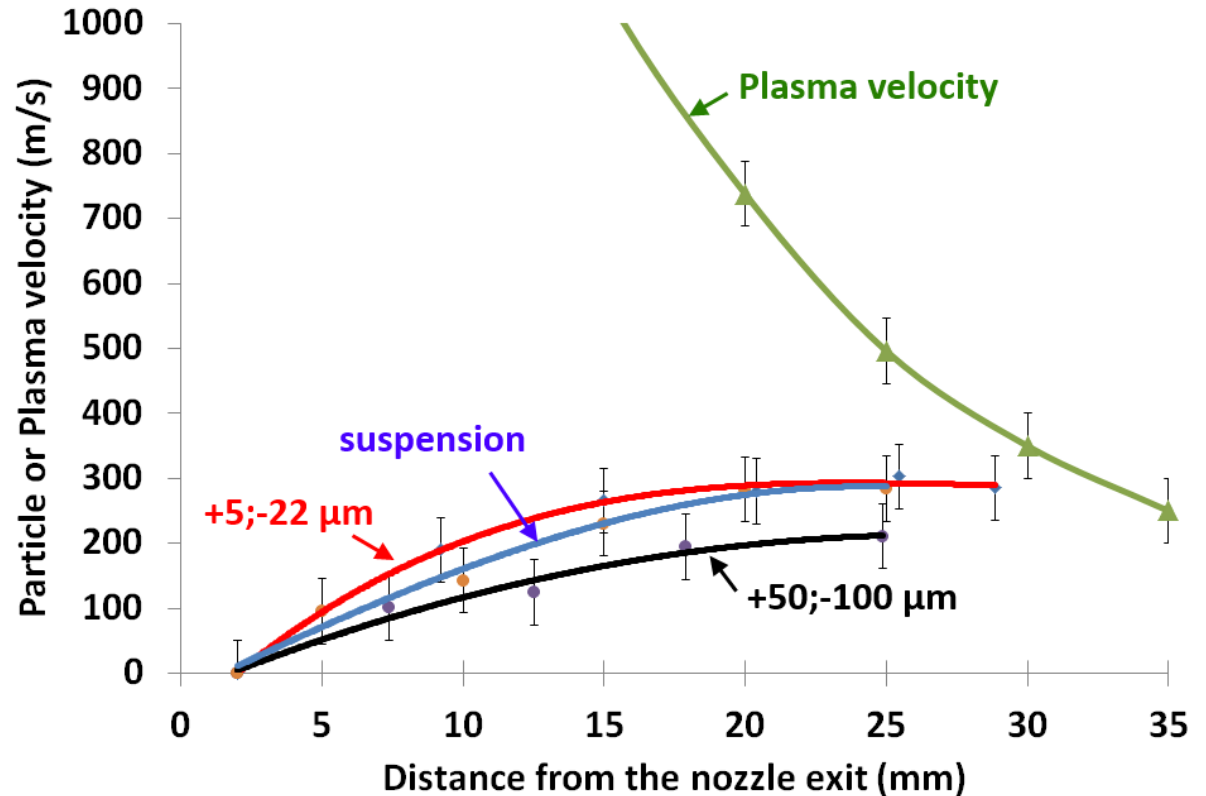
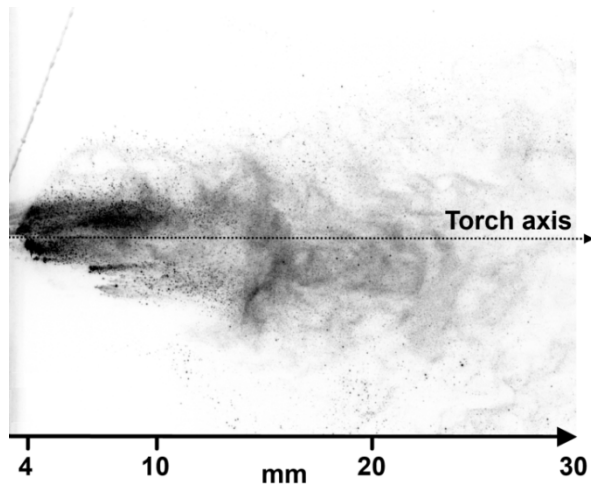
Projection plasma

Nombreuses présentations sur la projection de suspensions

Goutier et al (Limoges) : Droplet and Particle Acceleration in Suspension Plasma Spraying



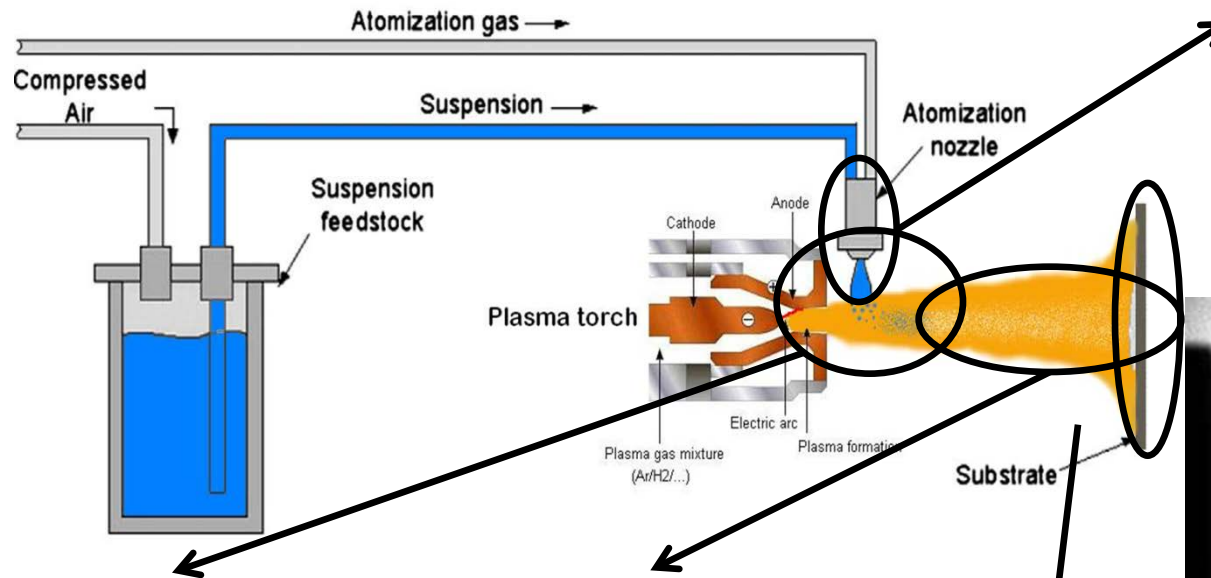
PIV



Ar: 45 slm, H₂: 3 slm, He: 45 slm
I = 600 A, h=11.5 MJ/kg

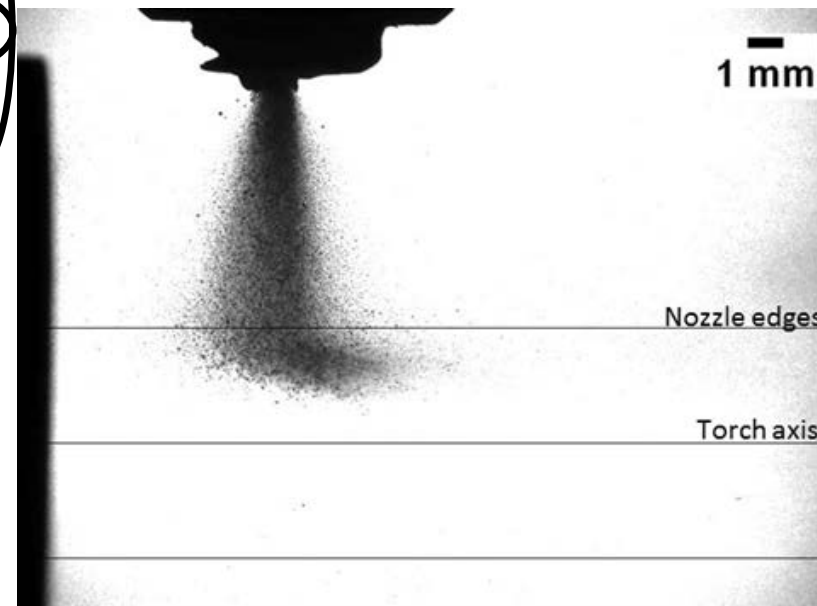
Projection plasma

Aubignat et al (UTBM) : Effect of suspension characteristics on in-flight particle properties and coating microstructures achieved by suspension plasma spray



1) Atomizer characterization

- spray geometry and width (shadowgraphy)
- droplet size measurements (laser diffraction)



2) Injection characterization (shadowgraphy)

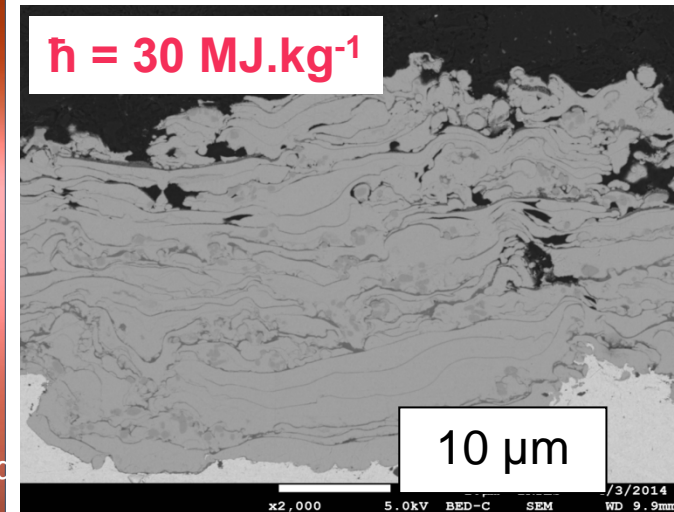
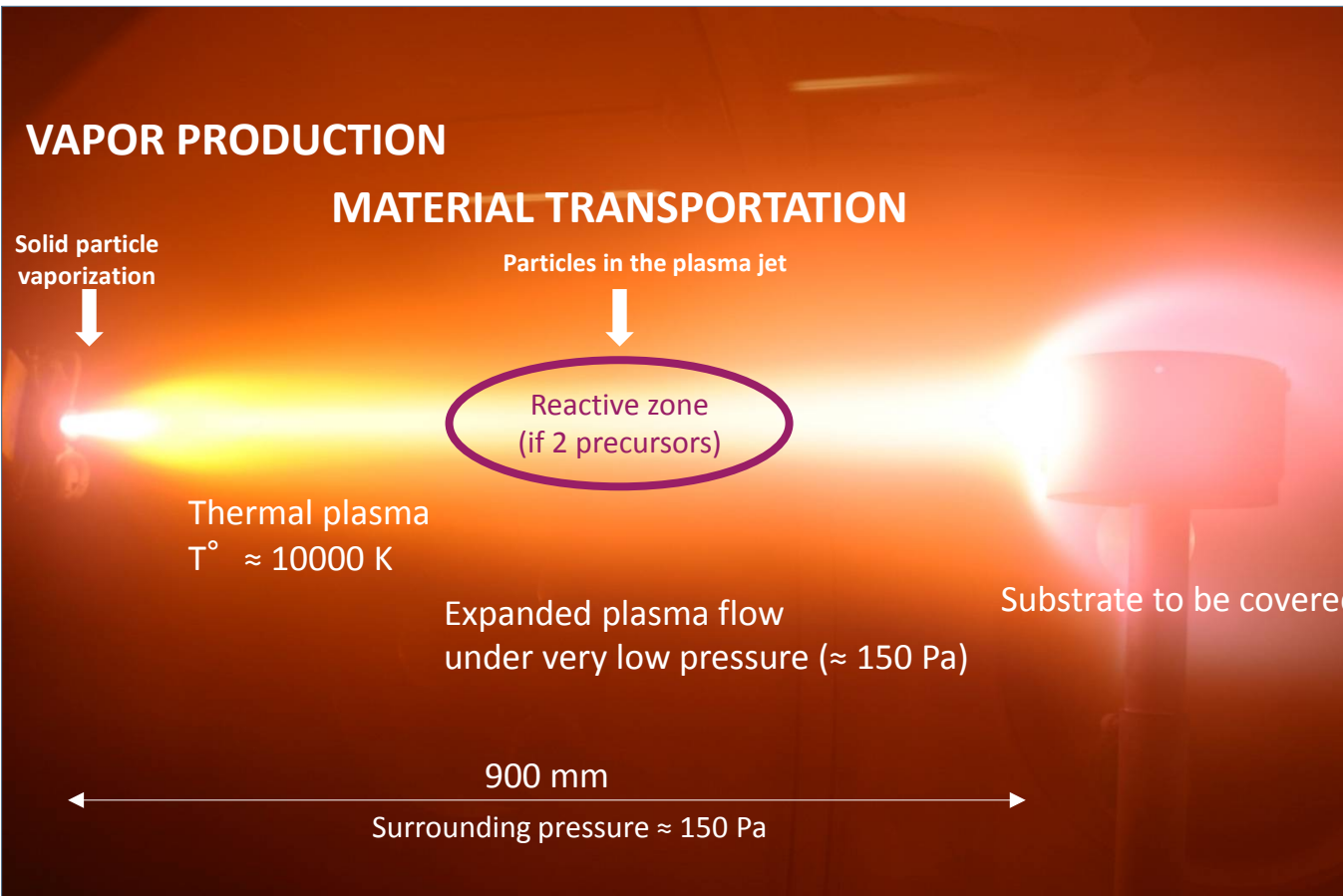
3) In-flight diagnosis:

- particle velocities (PIV)
- particle collection

4) Coating morphology observation (SEM)

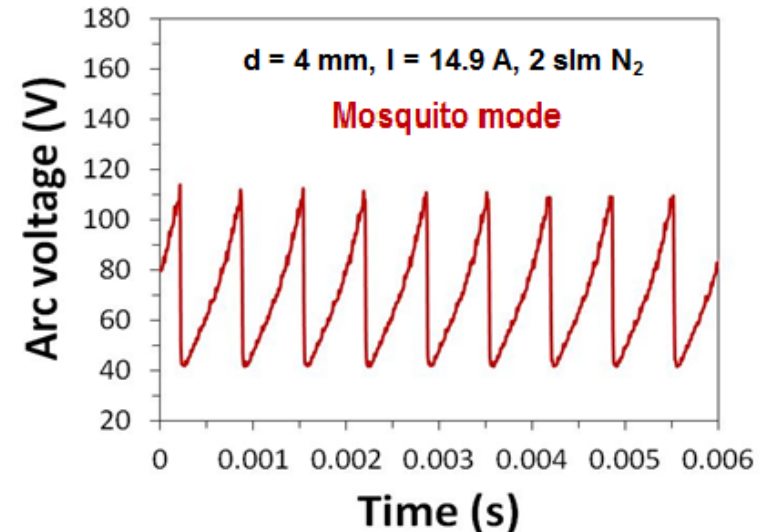
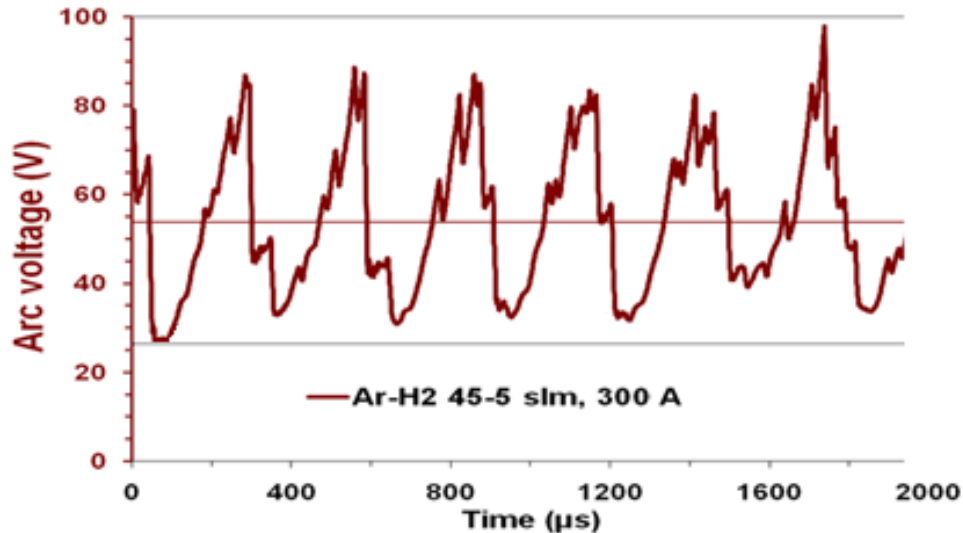
Projection plasma

Vautherin et al (UTBM) : Projection plasma réactive à très basse pression (150 Pa)
Matériaux non congruents (nitrures, carbures). Ici TiN_x



Projection plasma

Krowka et al (Limoges): Pulsed laminar arc jet with synchronized suspension injection-spectroscopic studies



Coupling Restrike and Helmholtz modes

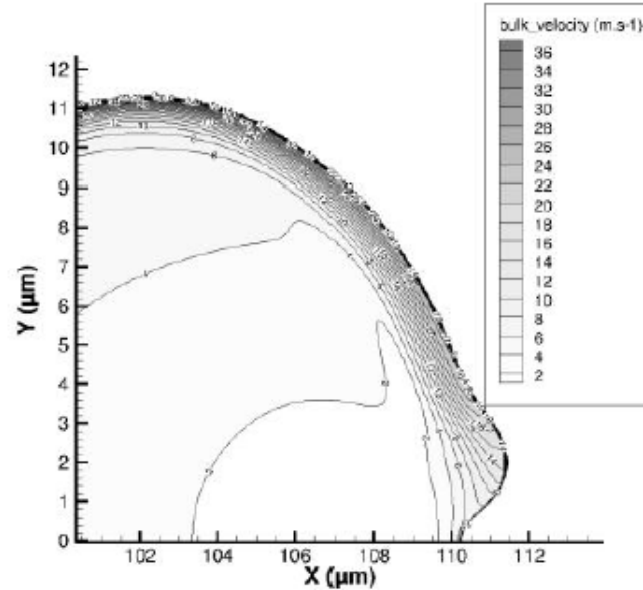
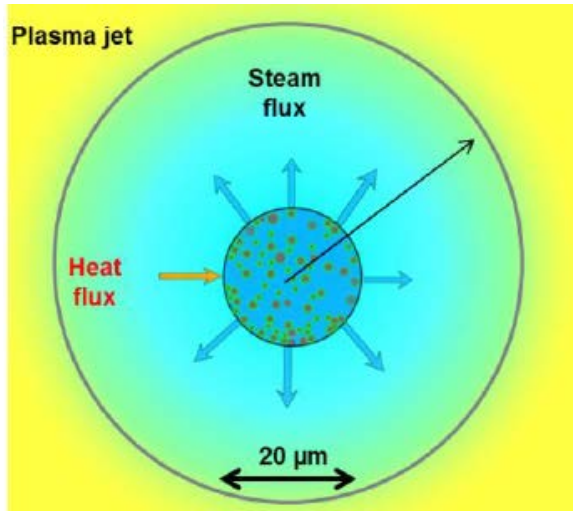


Mosquitorch

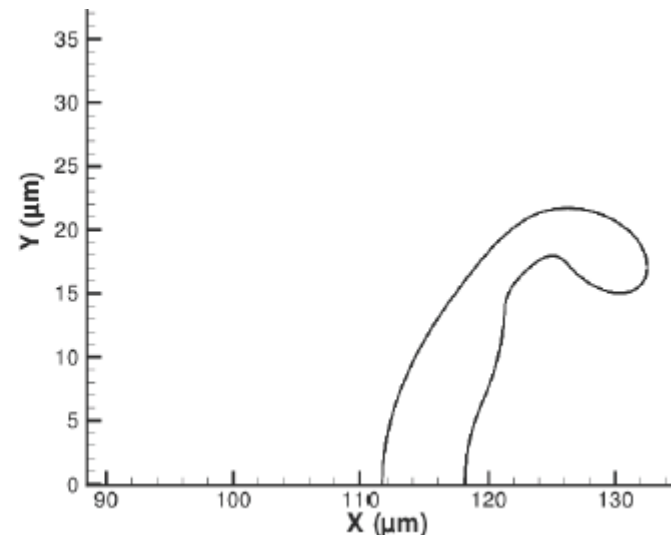
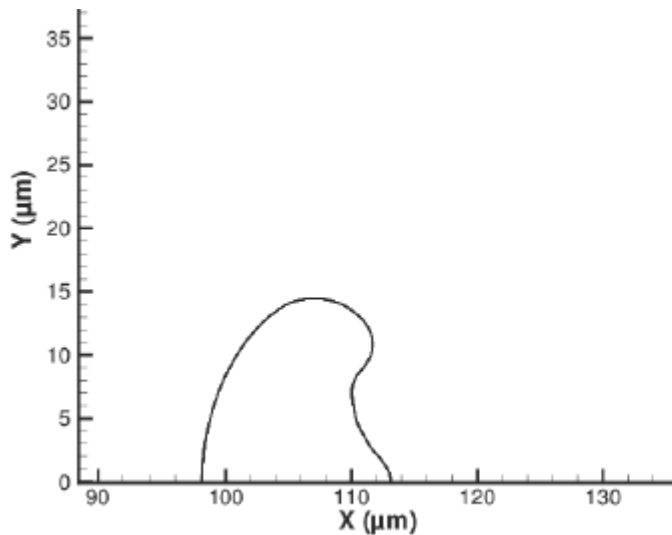
- ❖ Pulsed, laminar plasma jet with modulated enthalpy
- ❖ New injection system + injection of TiO₂ synchronized with the plasma
- ❖ + controlled and uniform treatment of the suspension

Projection plasma

Meillot et al (CEA) : Mechanisms of heat transfer between droplet and plasma jet in Suspension Plasma Spraying



Vitesse à l'intérieur de la gouttelette à 1 μs



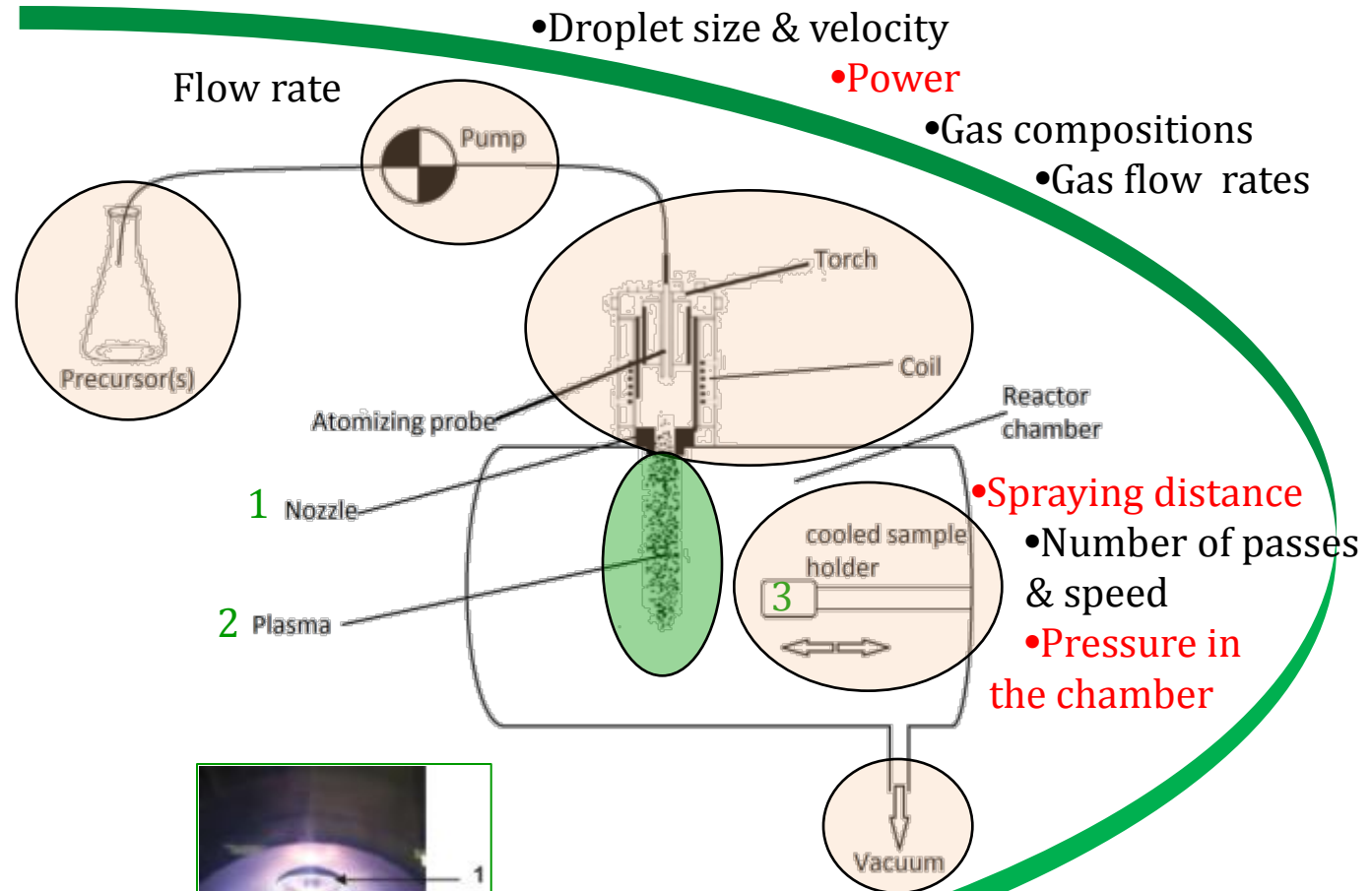
Forme de la gouttelette après 2,25 et 4,25 μs

Projection plasma par torche ICP

Faivre et al (Sherbrooke et CIRIMAT) : A study of the suspension induction plasma spraying parameters to reduce the decomposition of hydroxyapatite coatings

- Ca/P ratio
- Composition
- Solvent
- Solid load

*F. Gitzhofer, E. Bouyer,
M. Boulos, Suspension
Plasma Spraying US
Patent 5 609 921, 1997*



Characterization:

- XRD of the coating and Rietveld refinement
- XPS
- FTIR and RAMAN
- SEM of the surface and the section



Nombreux paramètres

Autres torches à plasma

1 Conf plénière + 1 conf invitée

Watanabe: Multi-phase AC arc for innovative glass melting

Autres torches à plasma

1 Conf plénière + 1 conf invitée

Watanabe: Multi-phase AC arc for innovative glass melting

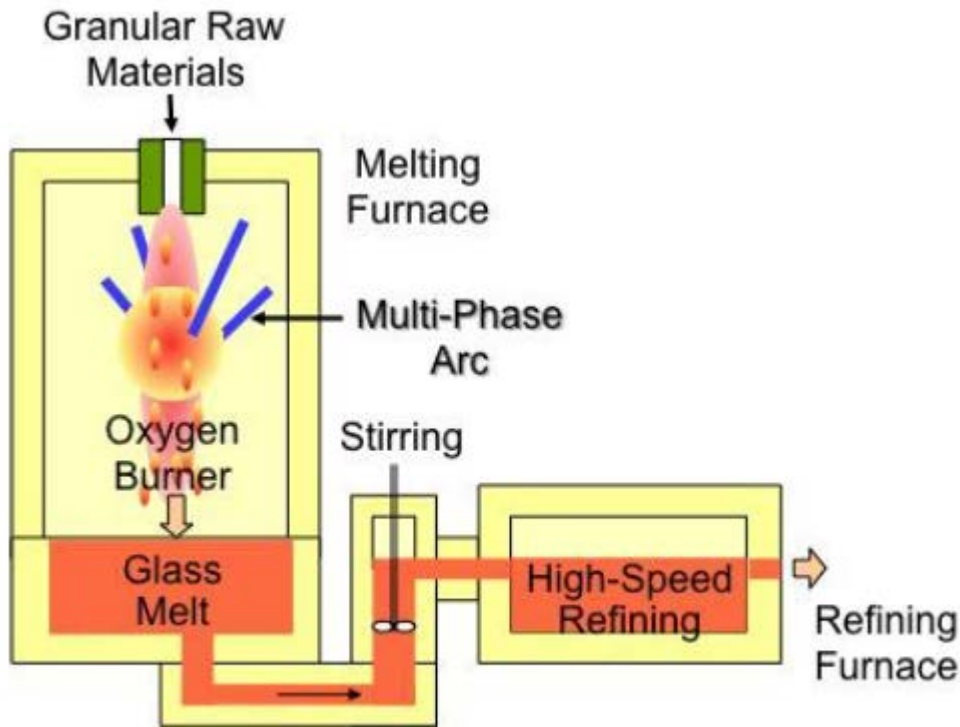


Figure 1. In-flight glass melting

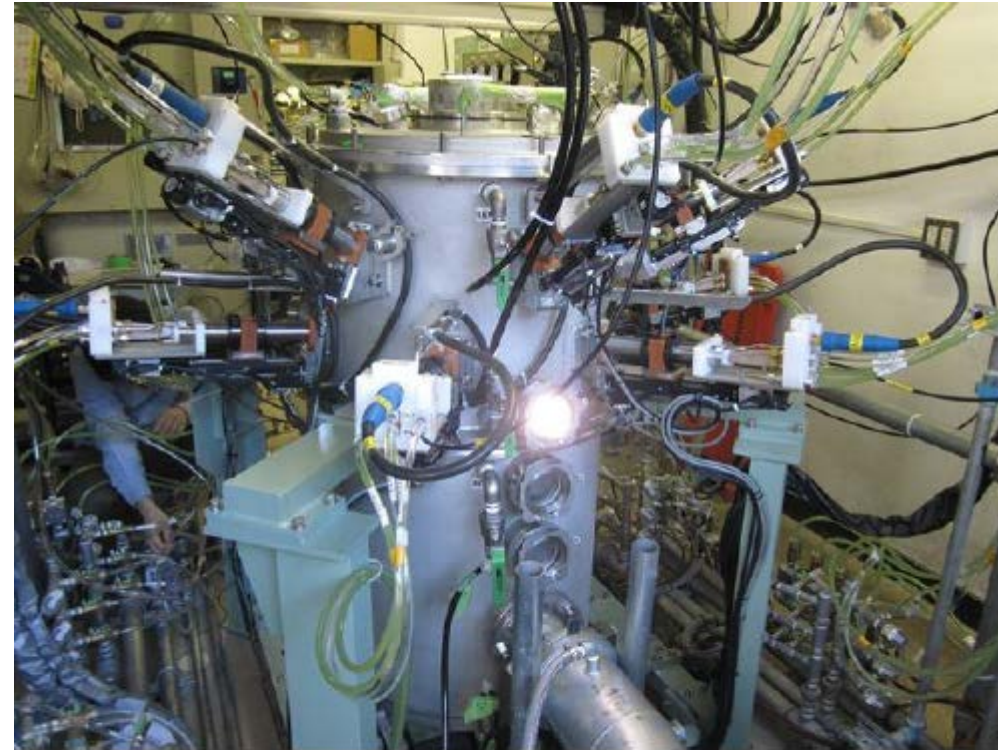
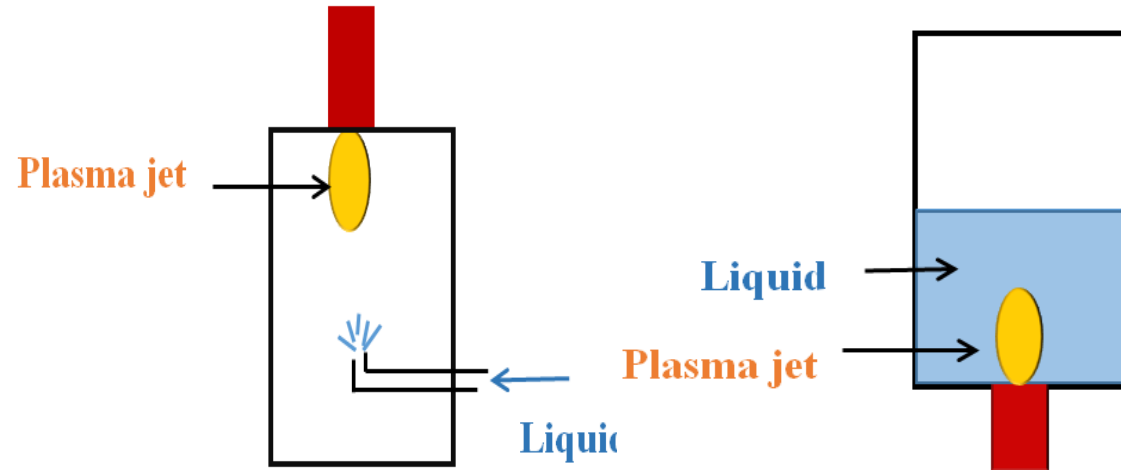


Figure 2. Multi-phase AC arc reactor

Autres torches à plasma

Soucy et al (Sherbrooke): Comparison of CO₂ and Oxygen Direct current (DC) Submerged Thermal Plasmas for Decomposition of Carboxylic Acid in Aqueous Solution

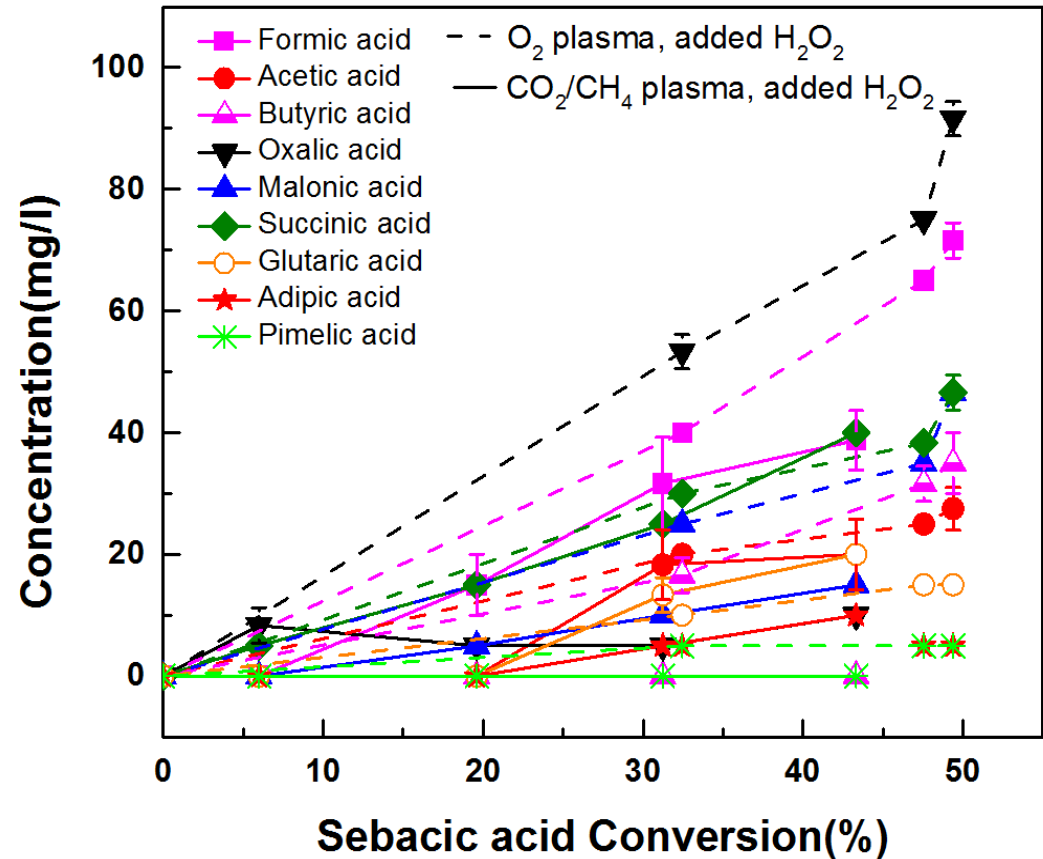
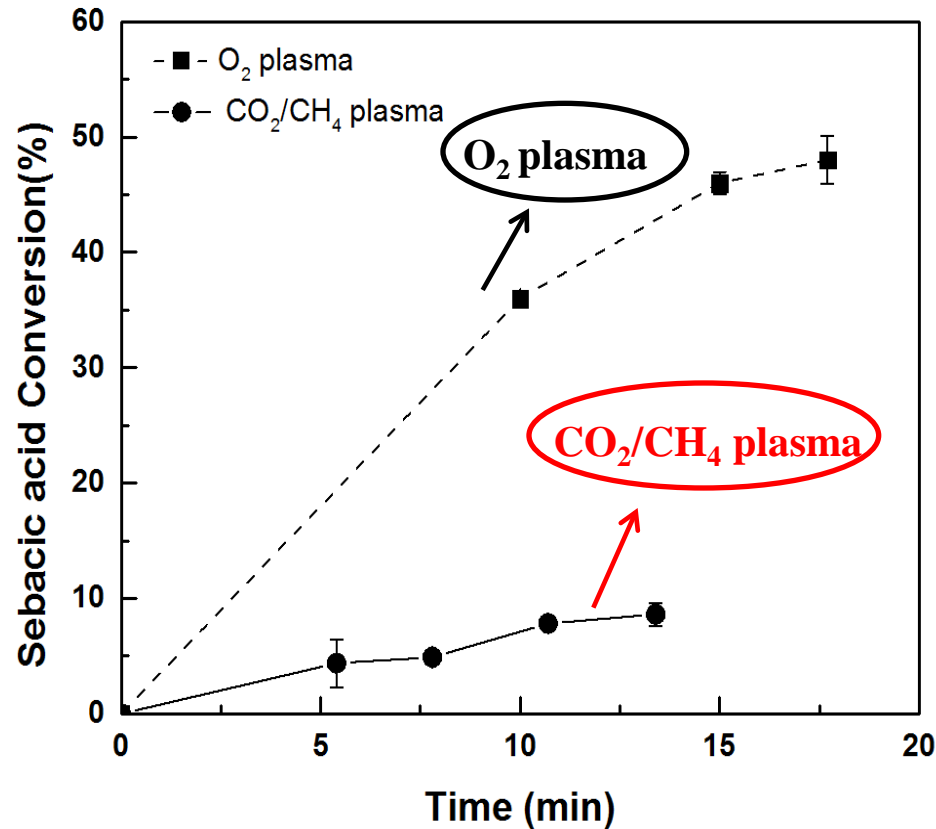


La 2^{ème} configuration est plus efficace

| Plasma gas | Plasma power (kW) | Gas ratio | Organic contaminant | Solution pH | Reactor pressure | Oxidizing agent |
|----------------------------------|-------------------|-----------|--|--------------|-------------------------|-------------------------------|
| Oxygen | 39 | - | Sebacic acid (C ₁₀ H ₁₈ O ₄) | 12.5 (basic) | Atmospheric and 1.7 atm | H ₂ O ₂ |
| CO ₂ /CH ₄ | 39 | 1.875 | Sebacic acid (C ₁₀ H ₁₈ O ₄) | 12.5 (basic) | Atmospheric and 1.7 atm | H ₂ O ₂ |

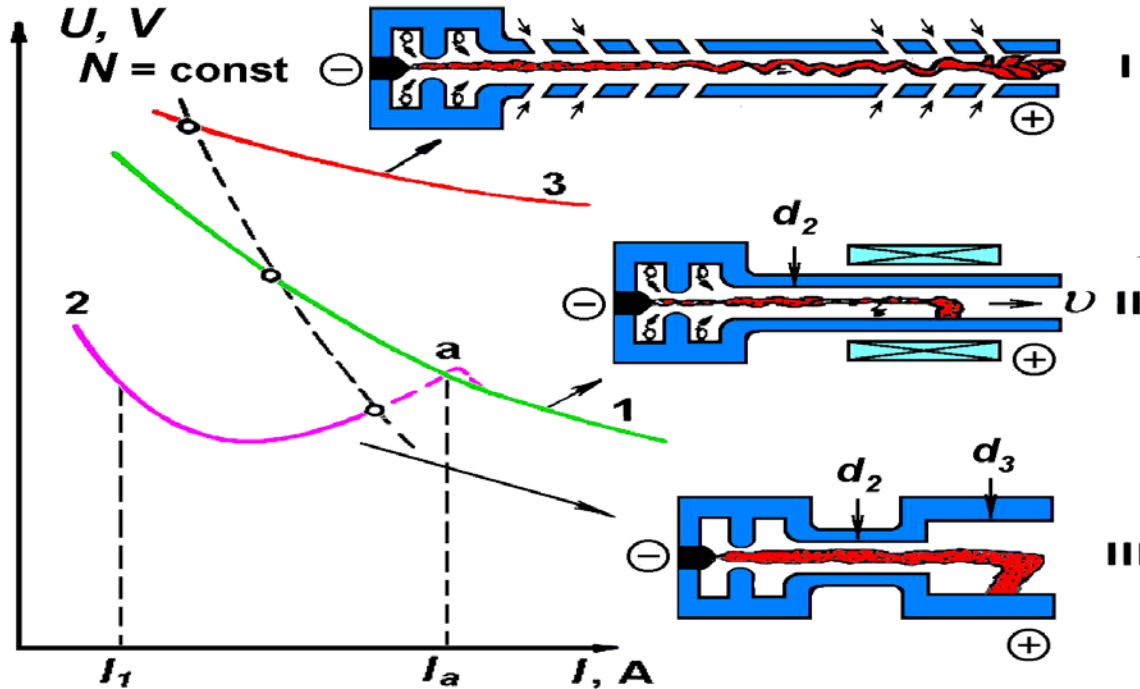
Autres torches à plasma

Soucy et al (Sherbrooke): Comparison of CO₂ and Oxygen Direct current (DC) Submerged Thermal Plasmas for Decomposition of Carboxylic Acid in Aqueous Solution



Autres torches à plasma

Torche à arc en cascade: Solonenko



Cascade torch with long arc

Torch with self-adjusting length of arc

Torch with arc length fixed by step



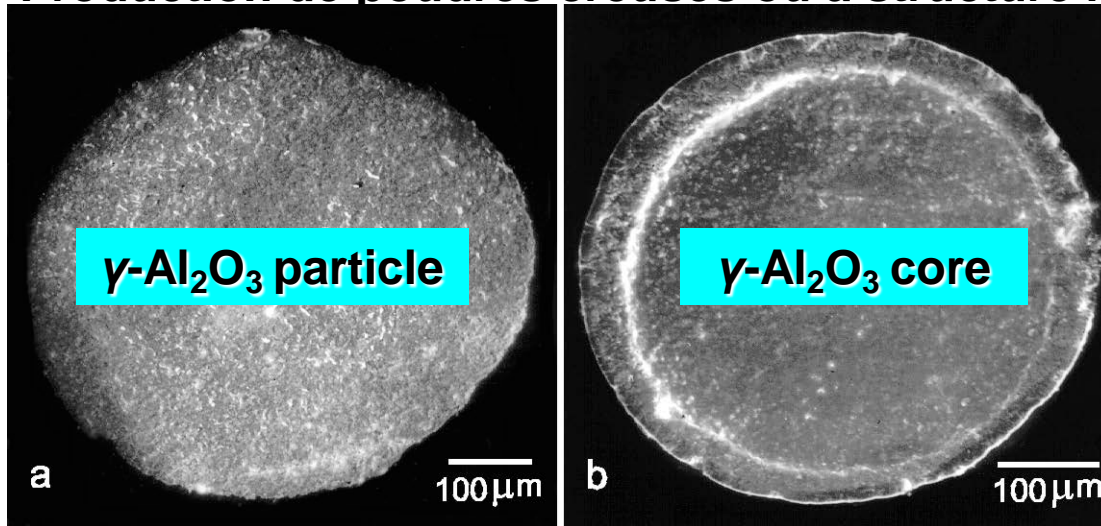
20-80 kW. Jets longs, quasi-laminaires ou turbulents suivant le débit (Ar-N₂)

Autres torches à plasma

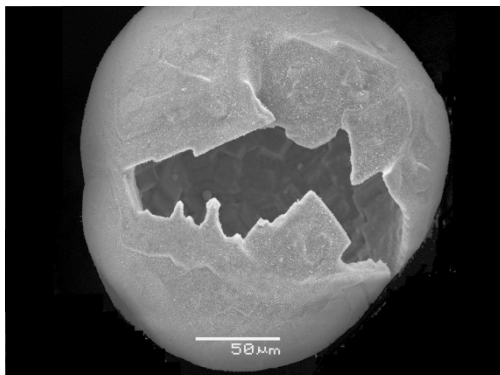
Torche à arc en cascade: Solonenko. Nombreux avantages: stabilité, flexibilité, gammes de puissance et enthalpie, longue durée de vie, haute efficacité.

Applications diverses montrées:

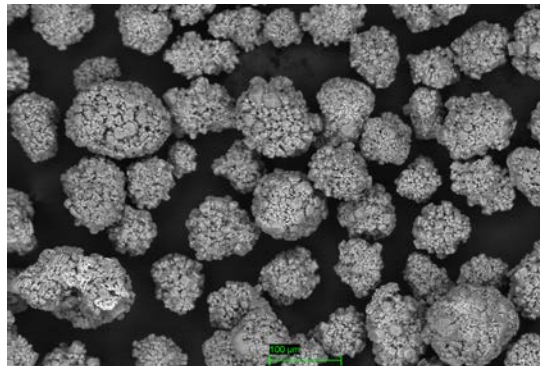
- Projection plasma Ni-Cr-B-C, Al_2O_3
- Sphéroidisation et traitements de poudres d'oxydes
- Production de poudres creuses ou à structure multi-échelle



Micrograph of a cross-section view of initial (a) and plasma-treated (b) Al_2O_3 particles.



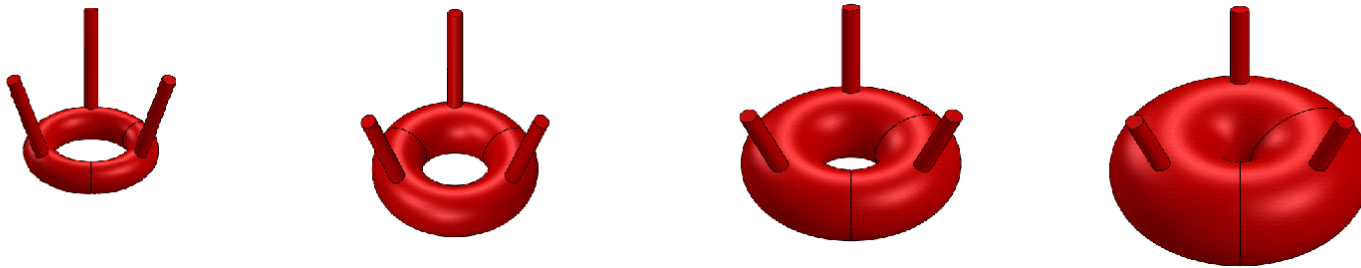
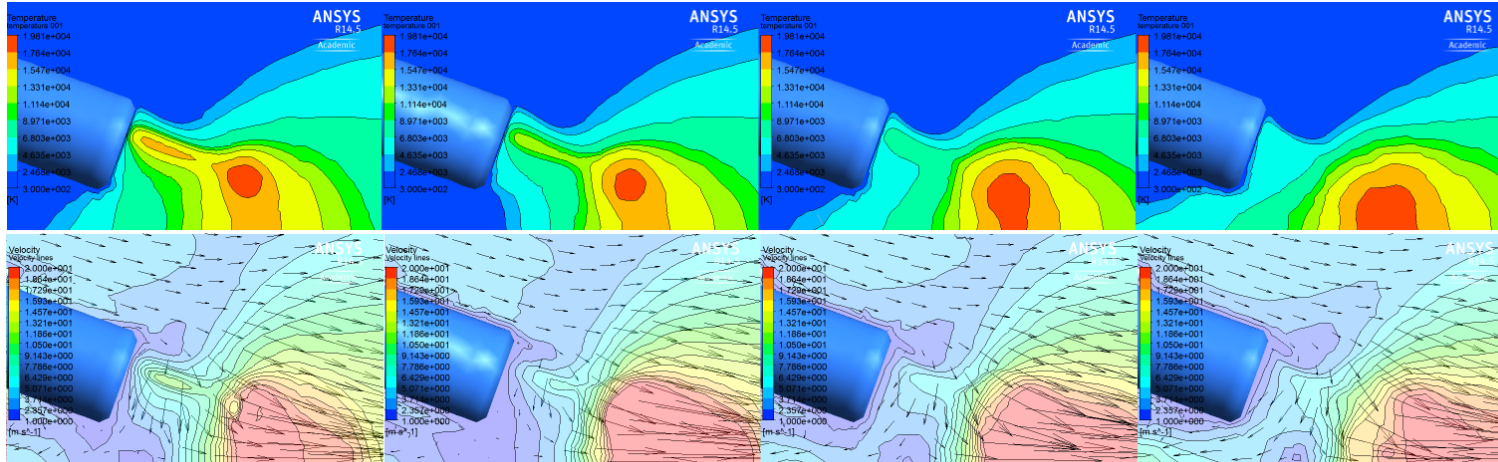
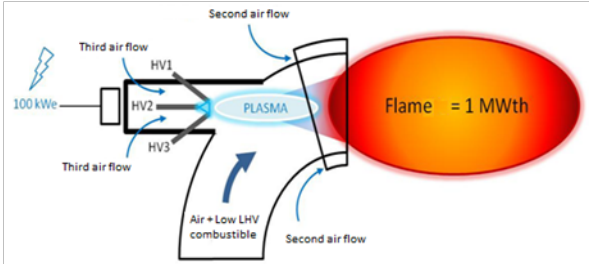
$\alpha\text{-Al}_2\text{O}_3$



Poudres catalytiques
 $\text{Al}_2\text{O}_3\text{-Cr}_2\text{O}_3$

Autres torches à plasma

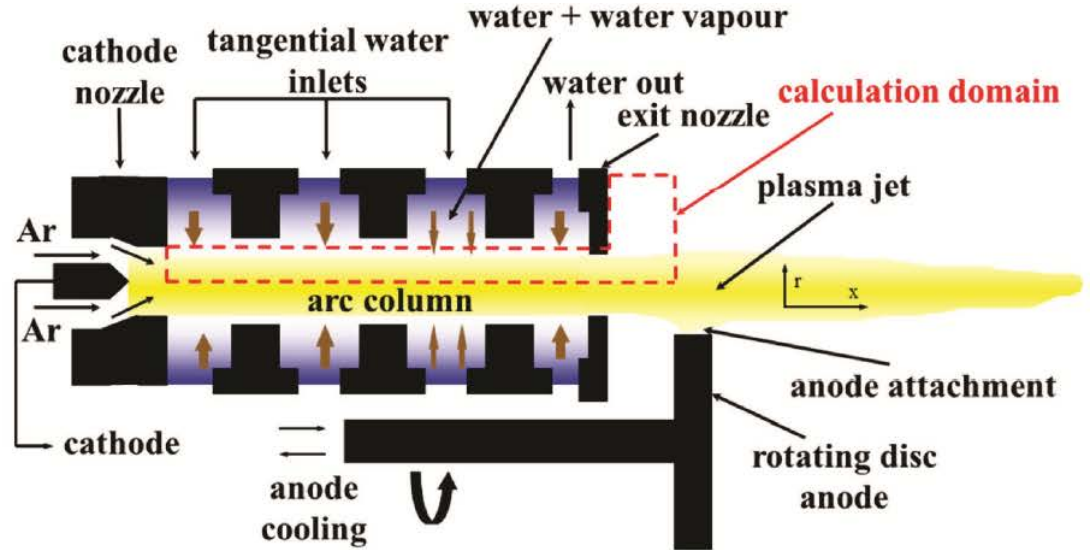
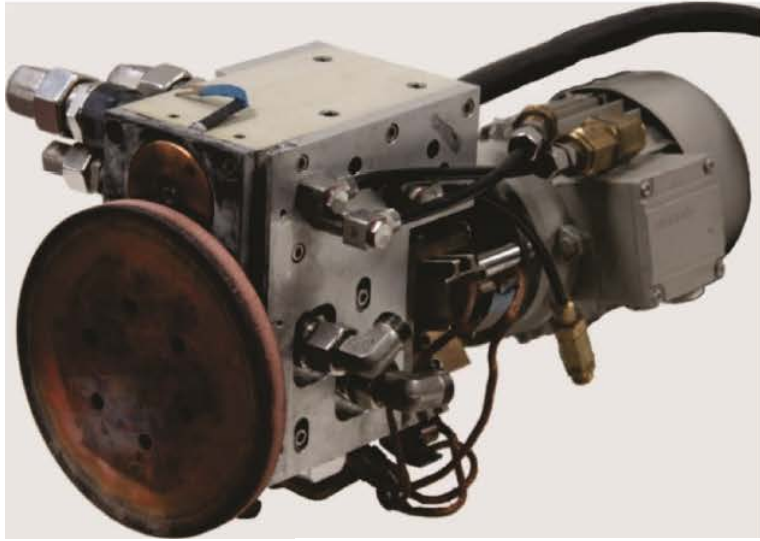
Torche AC triphasée 100 kW: Fulchéri et al. Air + Azote. Modèle Ansys



Temperature and velocity fields nearby the electrode tip (top) and arc column simplified shape (bottom) in 4 different volumes: 2 cm³, 4 cm³, 8 cm³ and 16 cm³

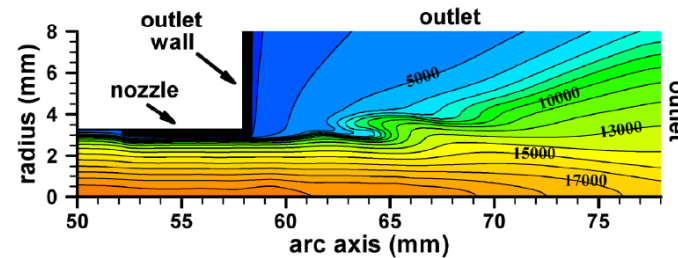
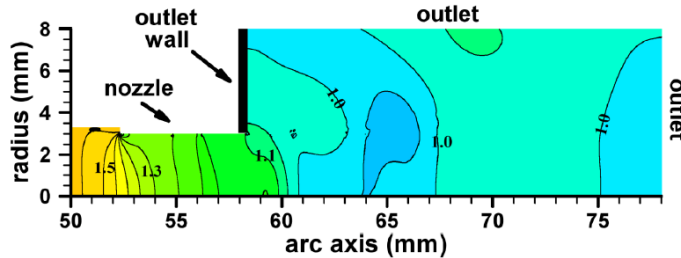
Autres torches à plasma

Torche hybride eau+Ar: Jenista et al (Prague). Modèle comparaison laminaire-turbulent



Laminar

Laminar

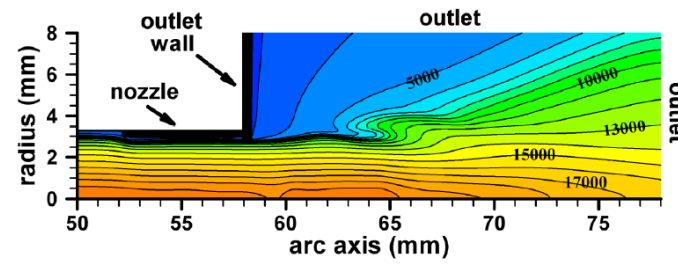
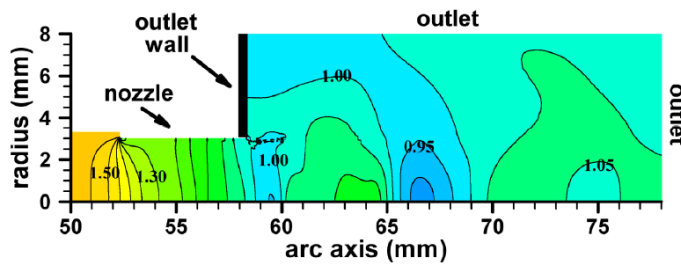


P (bar)

T (K)

Turbulent

Turbulent



Synthèse de poudres et nanomatériaux

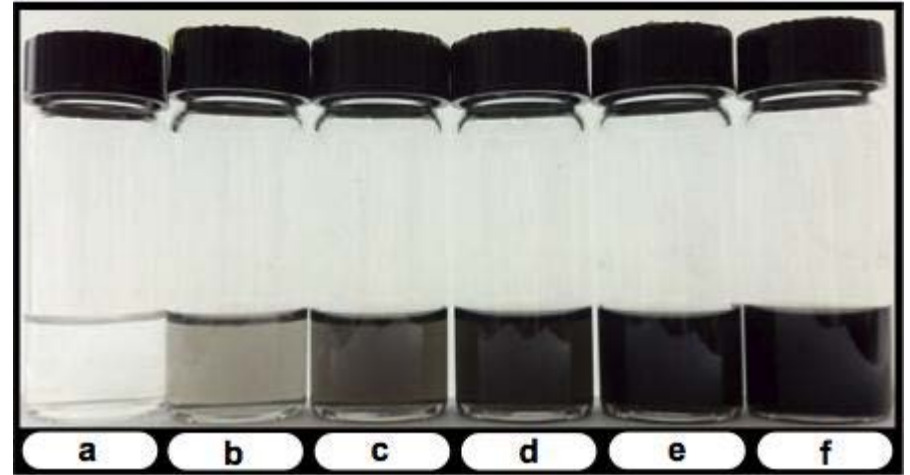
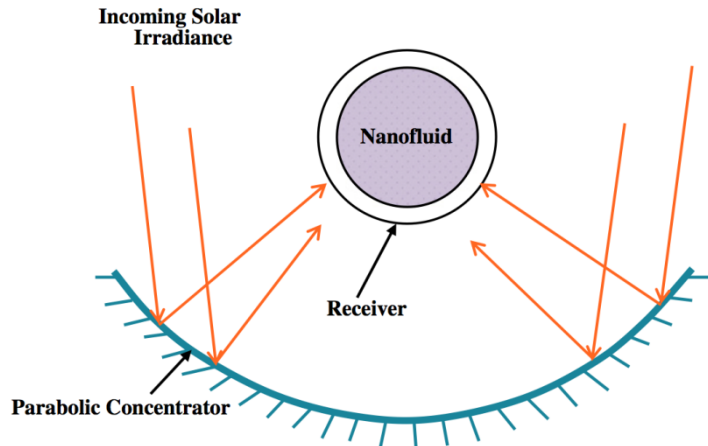
1 Conf plénière (Coulombe, McGill): Plasma-Assisted Synthesis of Nanostructures: A Key Enabler for Green Technologies

1 Conf invitée (Tanaka, Japon): Adoption of Pulse-Modulated Induction Thermal Plasmas with Time-Controlled Feedstock Feeding to High Production Rate Synthesis of Metallic Ion Doped TiO₂ Nanopowder

Synthèse de poudres et nanomatériaux

Conf plénière (Coulombe, McGill): Plasma-Assisted Synthesis of Nanostructures: A Key Enabler for Green Technologies. Revue bibliographique + résultats récents à McGill

nanofluid synthesis for solar thermal energy harvesting



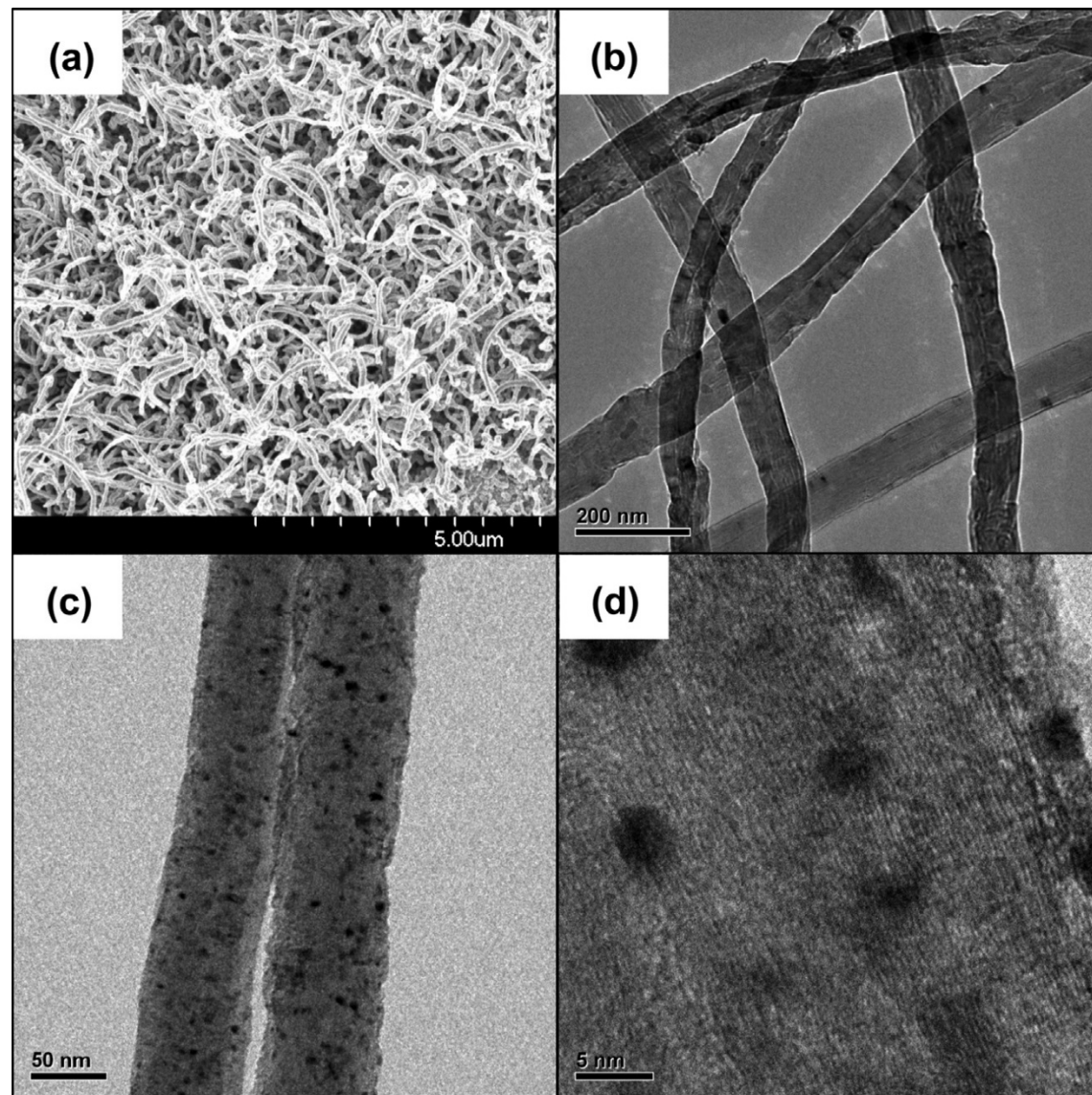
Various concentrations of ethylene glycol based CNT nanofluids, 3 months after synthesis

CNT produits par CVD à haute température et traités par décharge lumineuse sous forme de torche ICP

→ forte stabilité à haute température

Synthèse de poudres et nanomatériaux

Conf plénière (Coulombe, McGill)
Fabrication d'électrodes catalytiques pour la production d'hydrogène. A la base production de MWCNT (par CVD) recouverts de NP de Ni en utilisant l'ablation laser pulsée (PLA).

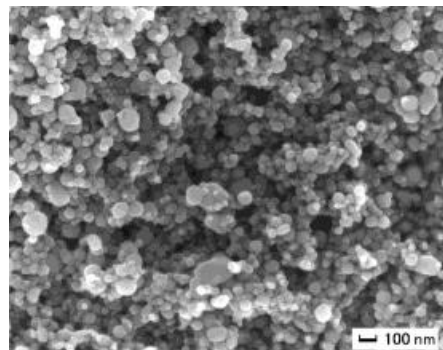
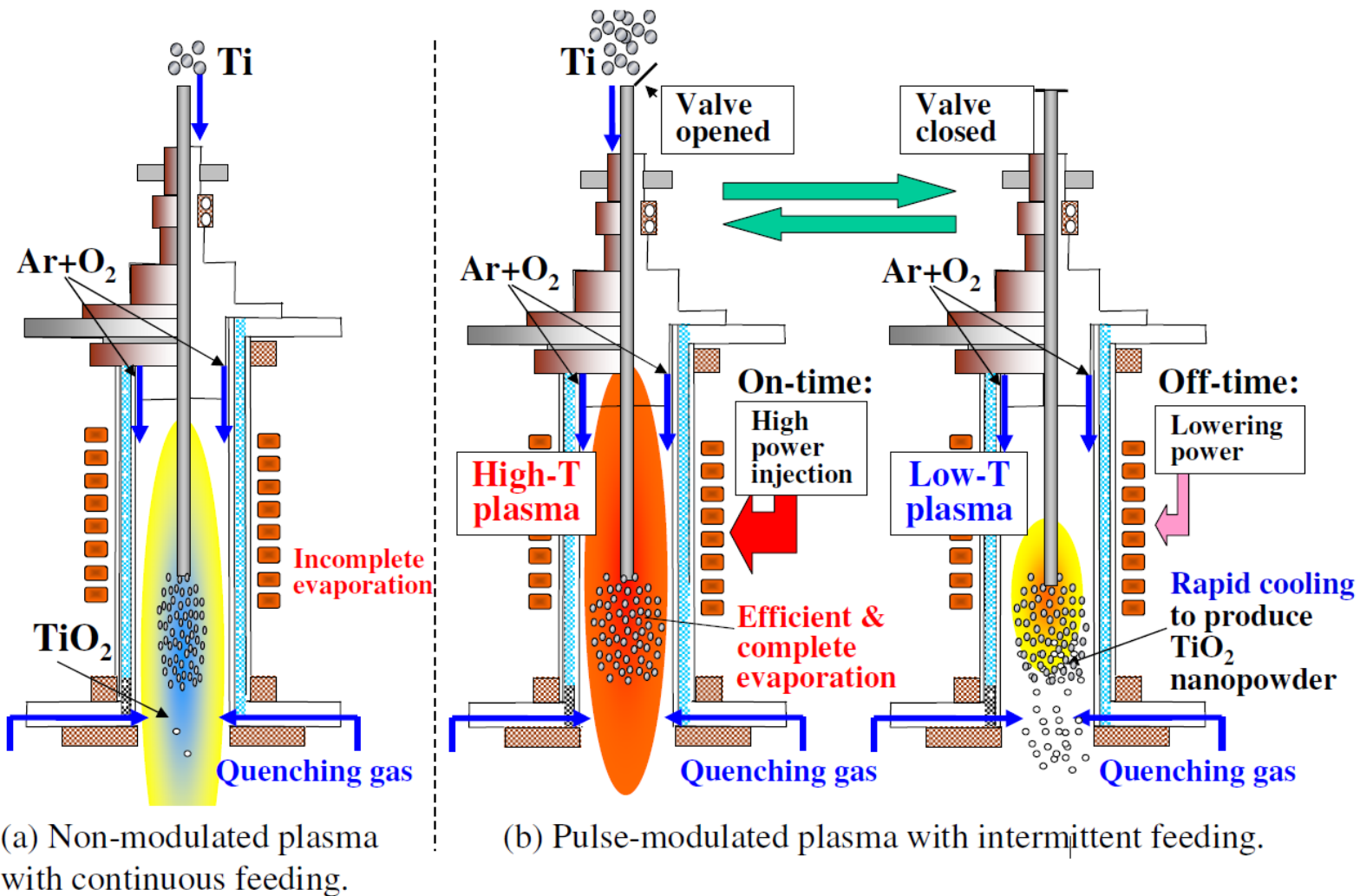


Micrographs displaying the nanostructured morphology of the Ni/MWCNT electrodes for various PLA times prior to electrochemical testing. (a) SEM image of Ni/MWCNT for 20 min PLA time, (b) TEM image of Ni/MWCNT for 0 min PLA time (control), TEM image of Ni/MWCNT for (c) 20 min PLA time, and (d) higher magnification of (c).

Synthèse de poudres et nanomatériaux

Conf invitée (Tanaka, Japon): Adoption of Pulse-Modulated Induction Thermal Plasmas with Time-Controlled Feedstock Feeding to High Production Rate Synthesis of Metallic Ion Doped TiO₂ Nanopowder

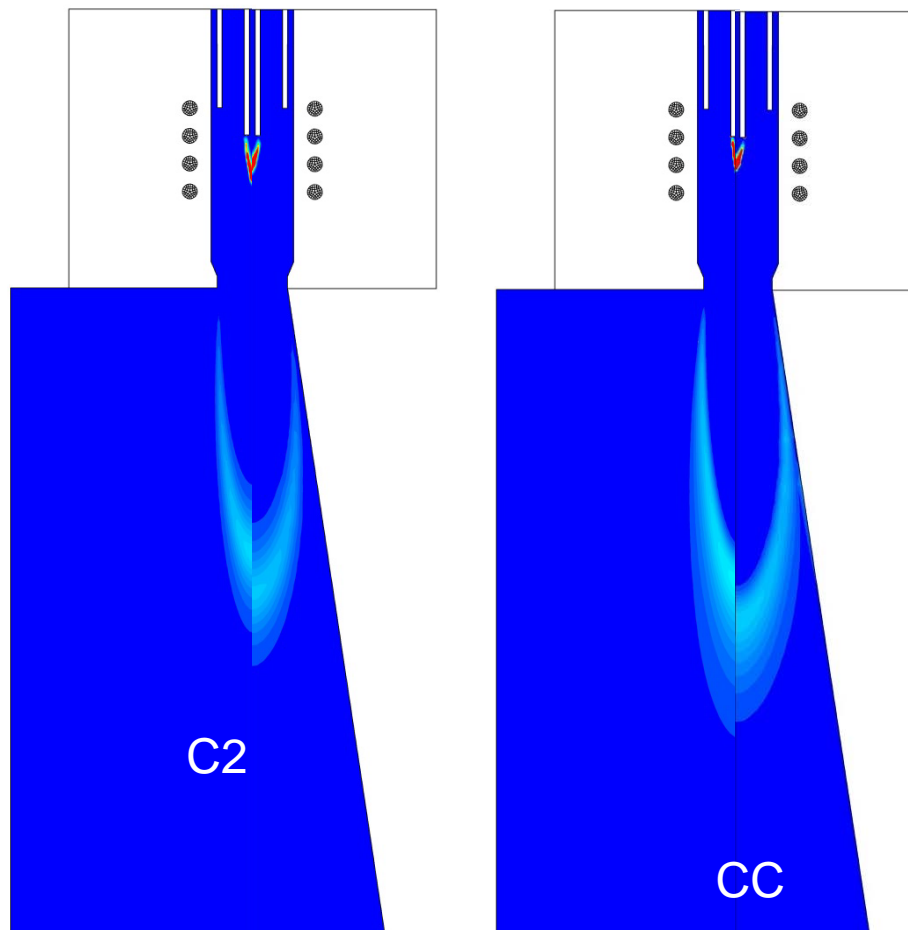
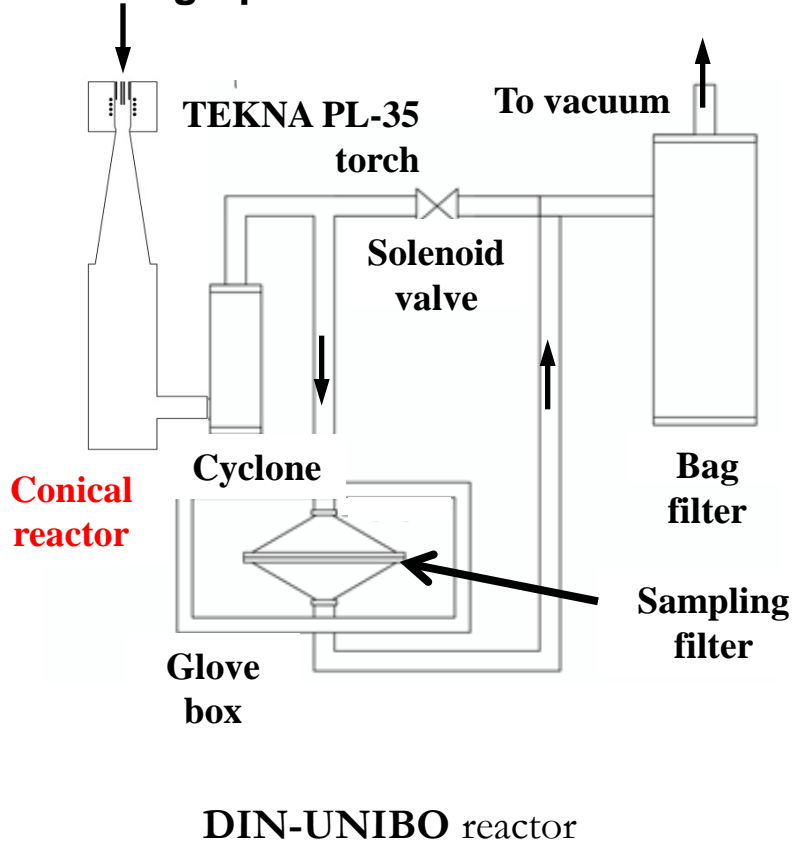
20 kW
450 kHz
90%Ar-10%O₂



Synthèse de poudres et nanomatériaux

Plusieurs papiers sur la synthèse de nanostructures de carbone:
Fullerènes par torche ICP (Bologne). Exp et modèle (fluide + cinétique)

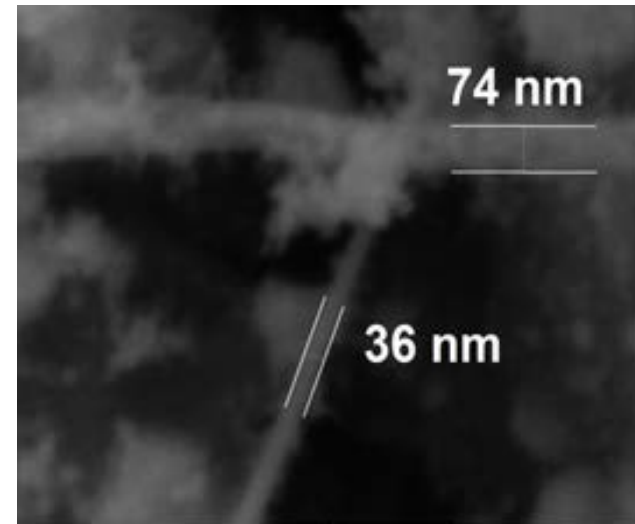
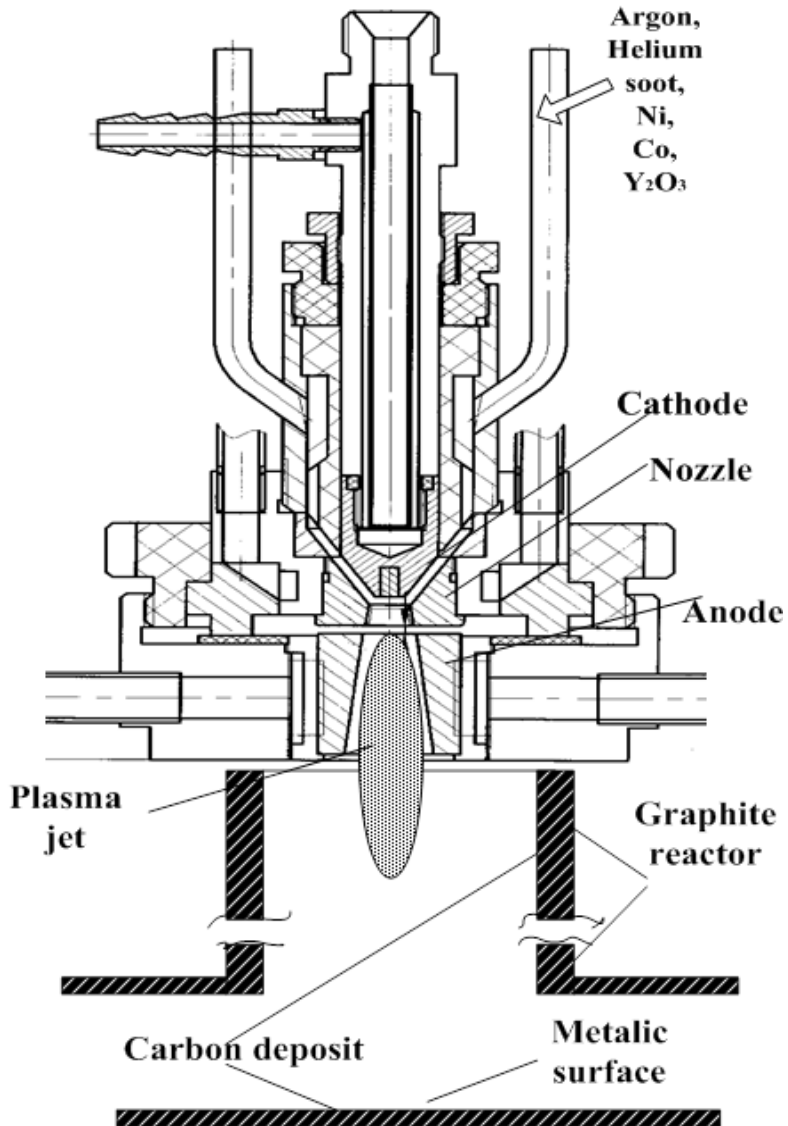
Poudres graphite



C vapour converted to C₂ and then to C₃ and CC
(molecules with 40 C atoms)

Synthèse de poudres et nanomatériaux

Plusieurs papiers sur la synthèse de nanostructures de carbone
CNT par torche avec anode divergente (Amirov, Russie). Objectif: forte production

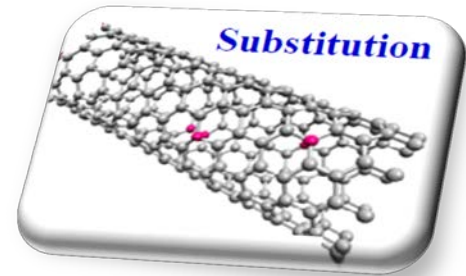


Diameter of carbon nanotubes changed from 16 to 74 nanometers depending on conditions.

Synthèse de poudres et nanomatériaux

Plusieurs papiers sur la synthèse de nanostructures de carbone

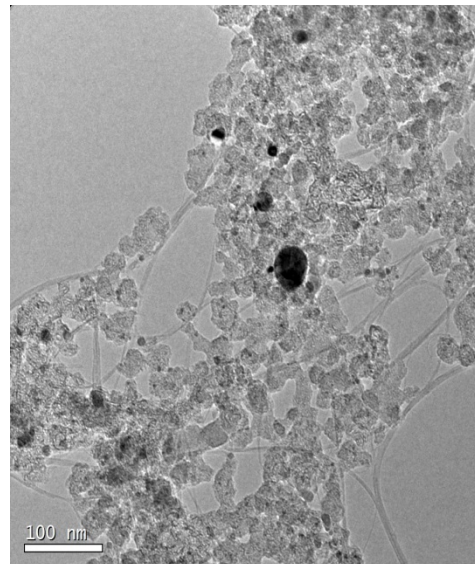
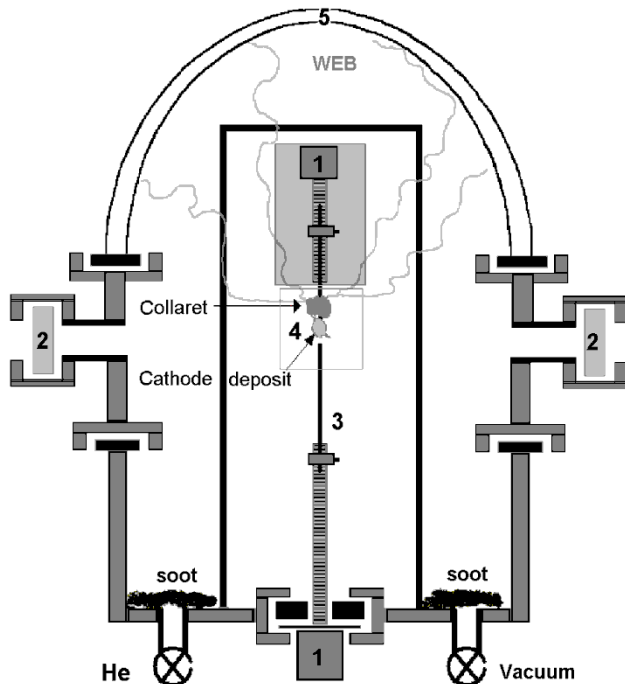
3) Substitution par B de SWNT (Laplace, CIRIMAT). NT metal ou semi-conducteur



| | | | | | |
|-------|-------|-------|-----|-----|----|
| | O | F | Ne | | |
| Al | S | P | Cl | Ar | |
| Ga | As | Se | Br | Kr | |
| In | Sn | Sb | Te | I | Xe |
| Tl | Pb | Bi | Po | At | Rn |
| Uuo | Uug | Uuh | Uus | Uuo | |
| 5 | 6 | 7 | | | |
| B | C | N | | | |
| 10.81 | 12.01 | 14.01 | | | |

Substitution: acceptor (**B**), donnor (**N**)
Sharp localized states above and below the Fermi level (n- or p-type doping) by substitution (removal of C atoms).

- Spectroscopie
- HRTEM, EXDS, **EELS**, XPS
- I=50-80 A, B (1,2,4 and 8 %)
- Gas (He –N₂ –Air), dopants nature



Most favorable case 80A :

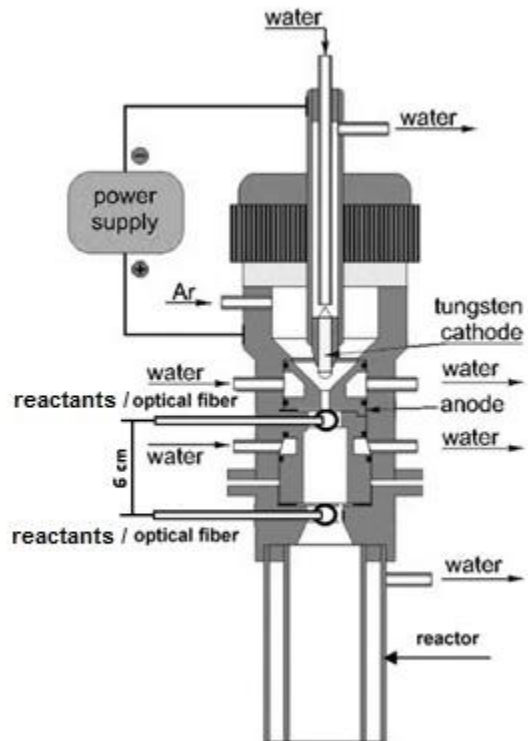
CB_x: 1,2%at Y ,2%B

CBN: N₂ ,1,2%at Y ,4%B

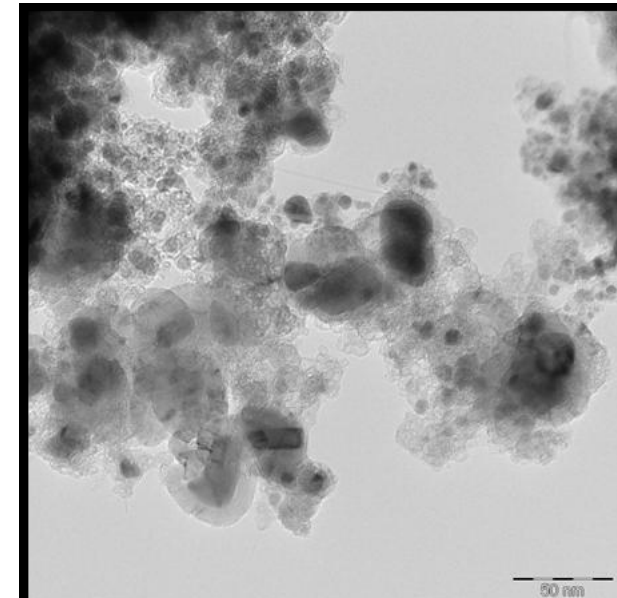
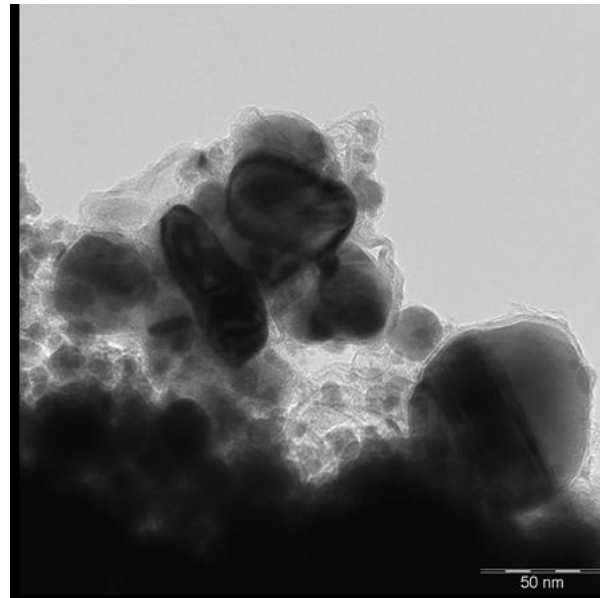
Doping confirmation (BN vs CBN).

Synthèse de poudres et nanomatériaux

Plusieurs papiers sur la synthèse de nanostructures de carbone:
2 papiers sur: carbon nanomaterials synthesis: carbon-encapsulated iron nanoparticles and few-layer graphene, by DC plasma torch. Lange et al (Varsovie)



- Spectroscopie d'émission optique sur différentes espèces pour obtenir des valeurs locales de température, densité électronique et concentration d'espèces
- Caractérisation des matériaux obtenus

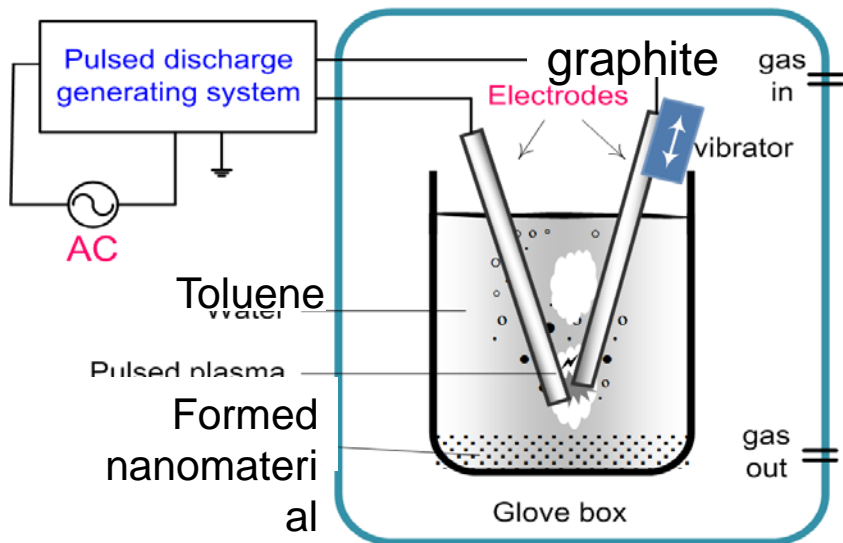


TEM images of products obtained from Fe and ethanol mixtures in two different ratios: A – $m\text{Fe}/m\text{EtOH} < 0.1$ and B - $m\text{Fe}/m\text{EtOH} > 0.1$

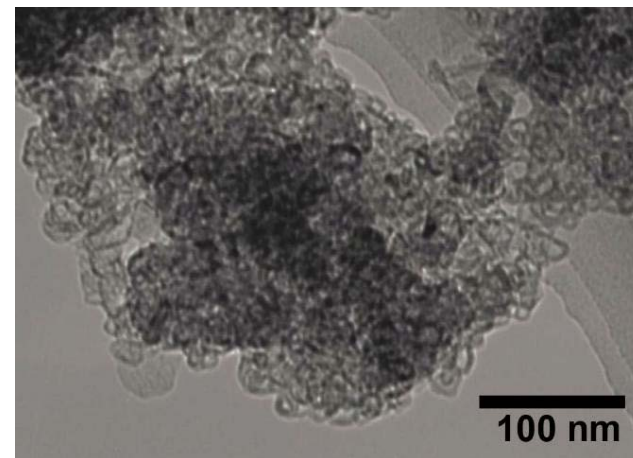
Synthèse de poudres et nanomatériaux

Plusieurs papiers sur la synthèse de nanostructures de carbone:

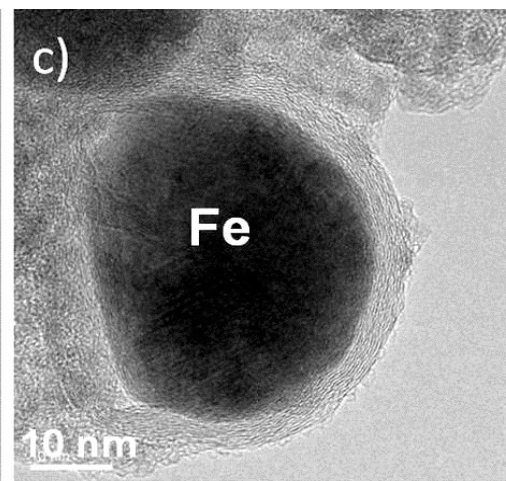
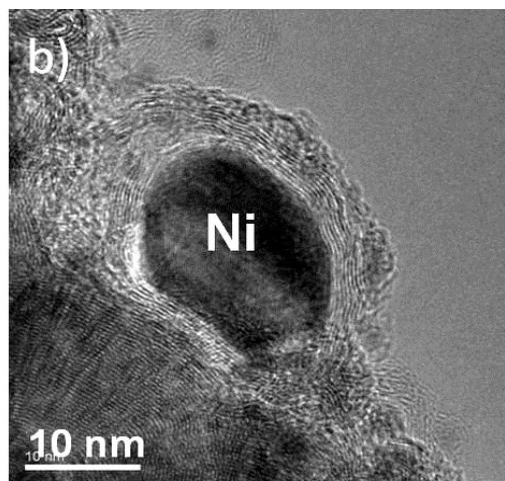
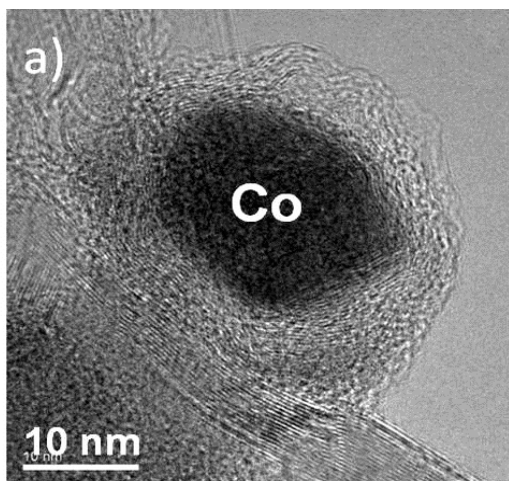
Effect of pulse duration and liquid type to formation of hollow carbon nano-onions by the pulsed plasma in liquid (Japon)



V: 0 – 200 V ; I: ~2 A
Pulse duration: 10 μ s

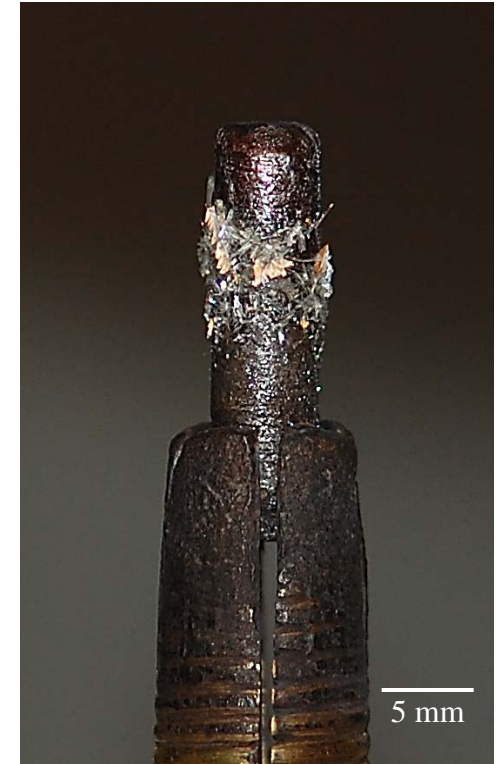
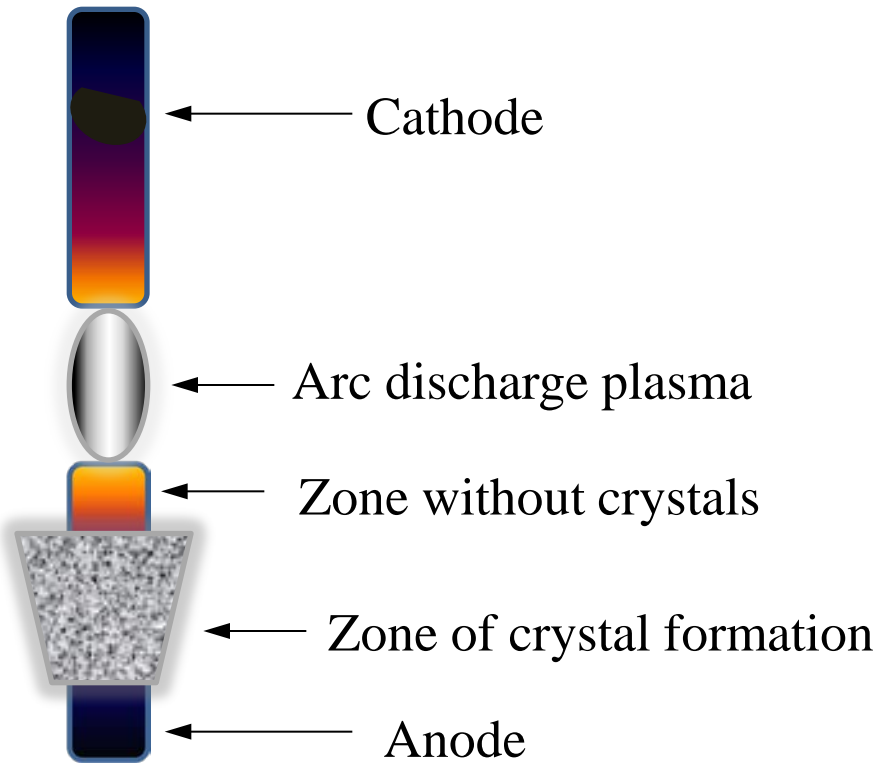


Graphite + metal \rightarrow **Metals encapsulated in carbon nano-onions Me@C**



Synthèse de poudres et nanomatériaux

Plusieurs papiers sur la synthèse de nanostructures de carbone:
Thermal plasma source for processing of MoO_3 crystals. Veklich (Ukraine)



The vertically oriented free-burning DC arc was ignited in air between the end surfaces of metallic molybdenum non-cooled electrodes.

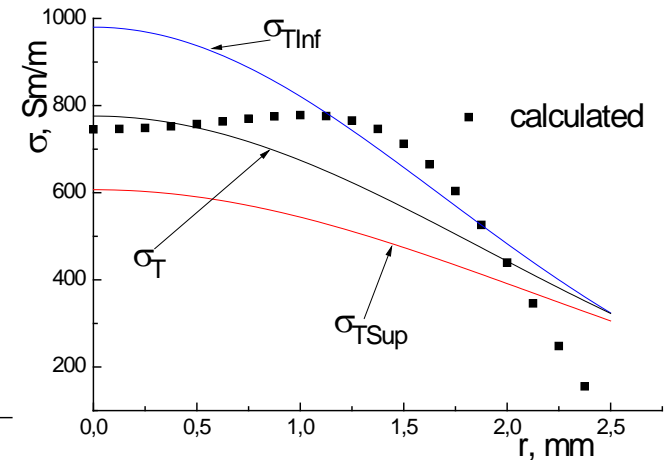
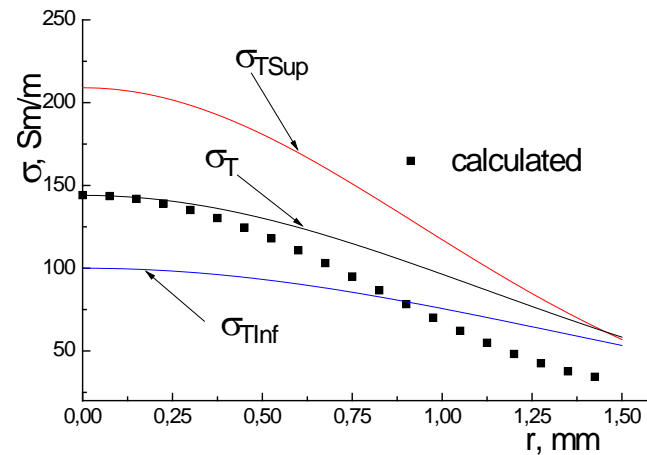
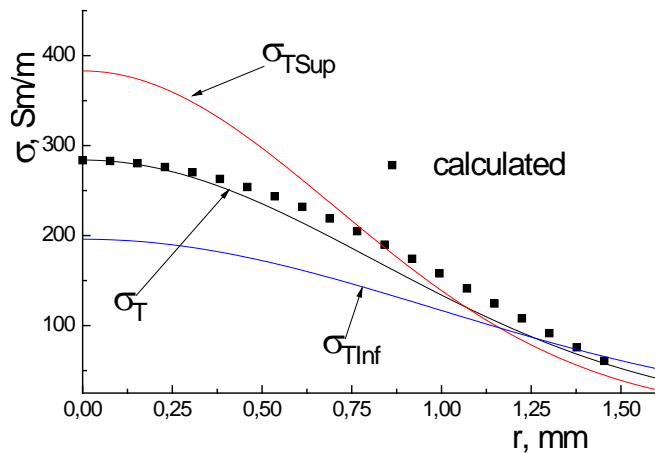
$\phi = 6$ mm; $d = 8$ mm; $I = 3,5$ A

Orthorhombic α - MoO_3 phase and only slight admixture of monoclinic β - MoO_3 phase

Propriétés des plasmas thermiques et quasi-thermiques

A l'équilibre qqs communications sur les propriétés de:

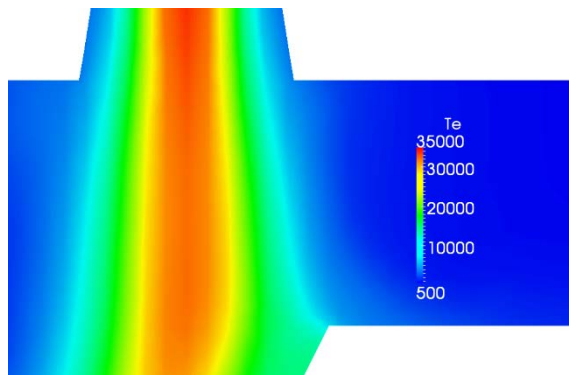
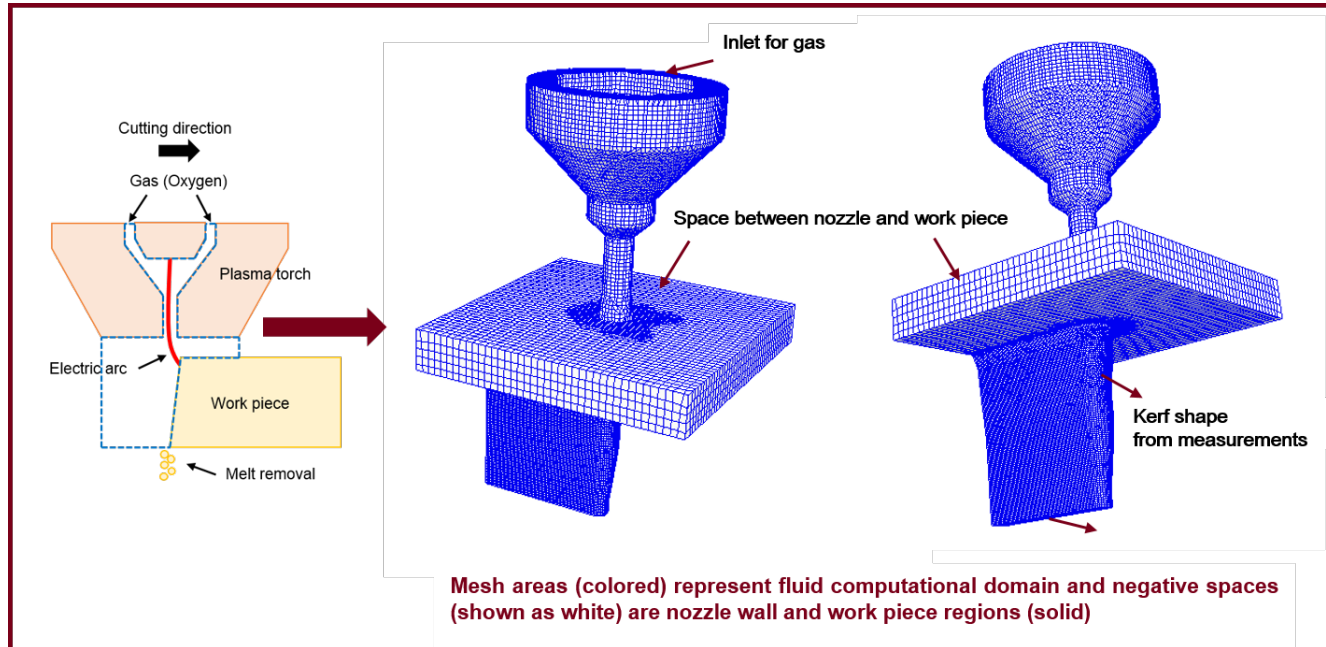
- SF₆ + PTFE + Cu et lois de mélanges
- CO₂ + air
- Ar + H₂O rayonnement
- Air + C + Cu (exp)
- Ar + (Ca, Na, W) pour lampes



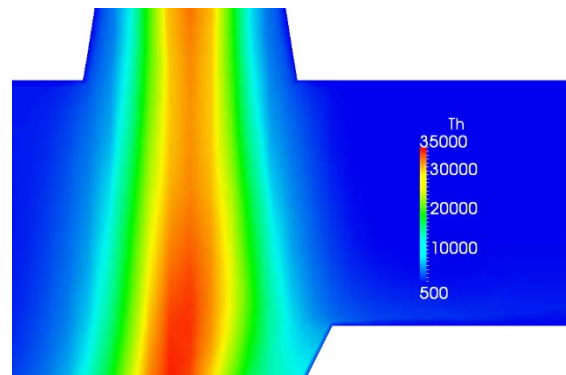
Radial profiles of electrical conductivity calculated from equation (2) and approximation curves σ_T , σ_{TSup} and σ_{TInf} in discharge gap of electric arcs between Cu-C electrodes at current 3.5 A in air (a) and between copper electrodes in air flow at currents 3.5 A (b) and 30 A (c)

Propriétés des plasmas thermiques et quasi-thermiques (2T)

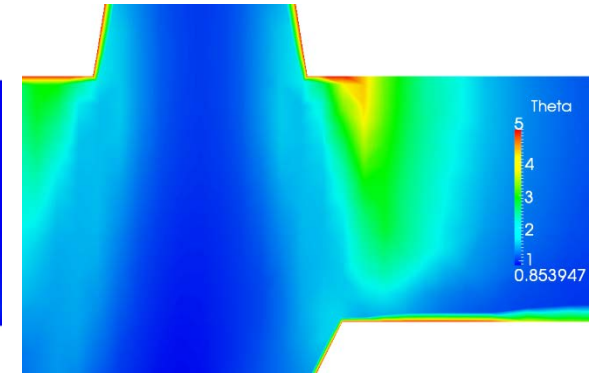
Modélisation 2T de la région anodique en découpe (Minneapolis)



Electron temperature, T_e [K]



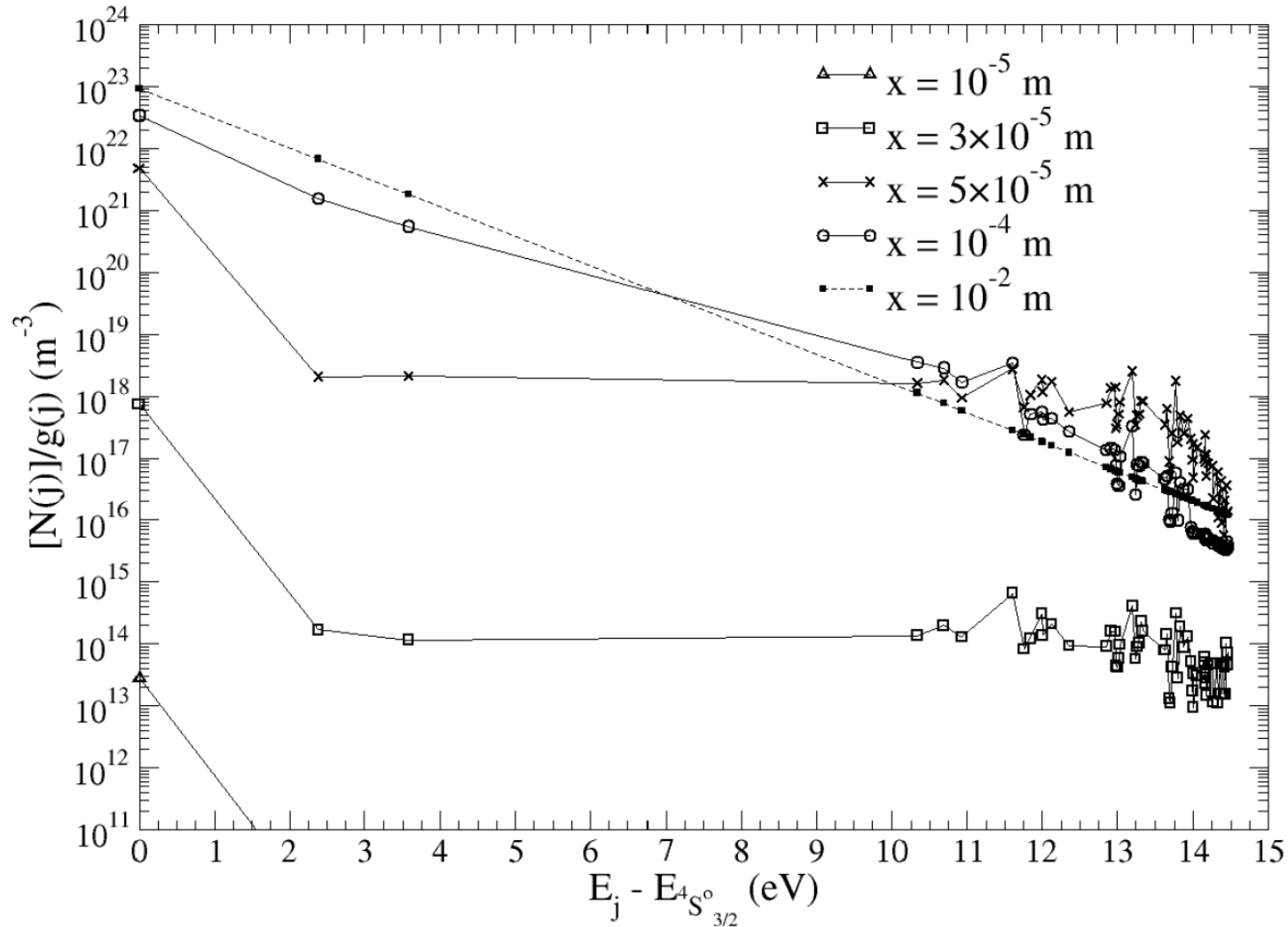
Heavy species temperature, T_h [K]



θ (T_e/T_h)

Propriétés des plasmas thermiques et quasi-thermiques

Modèles collisionnels-radiatifs pour rentrées martiennes (Bultel, Rouen): azote et air



Propriétés des plasmas thermiques et quasi-thermiques

Très intéressant: transfert radiatif dans un plasma moléculaire à 2T (Soufiani et al)

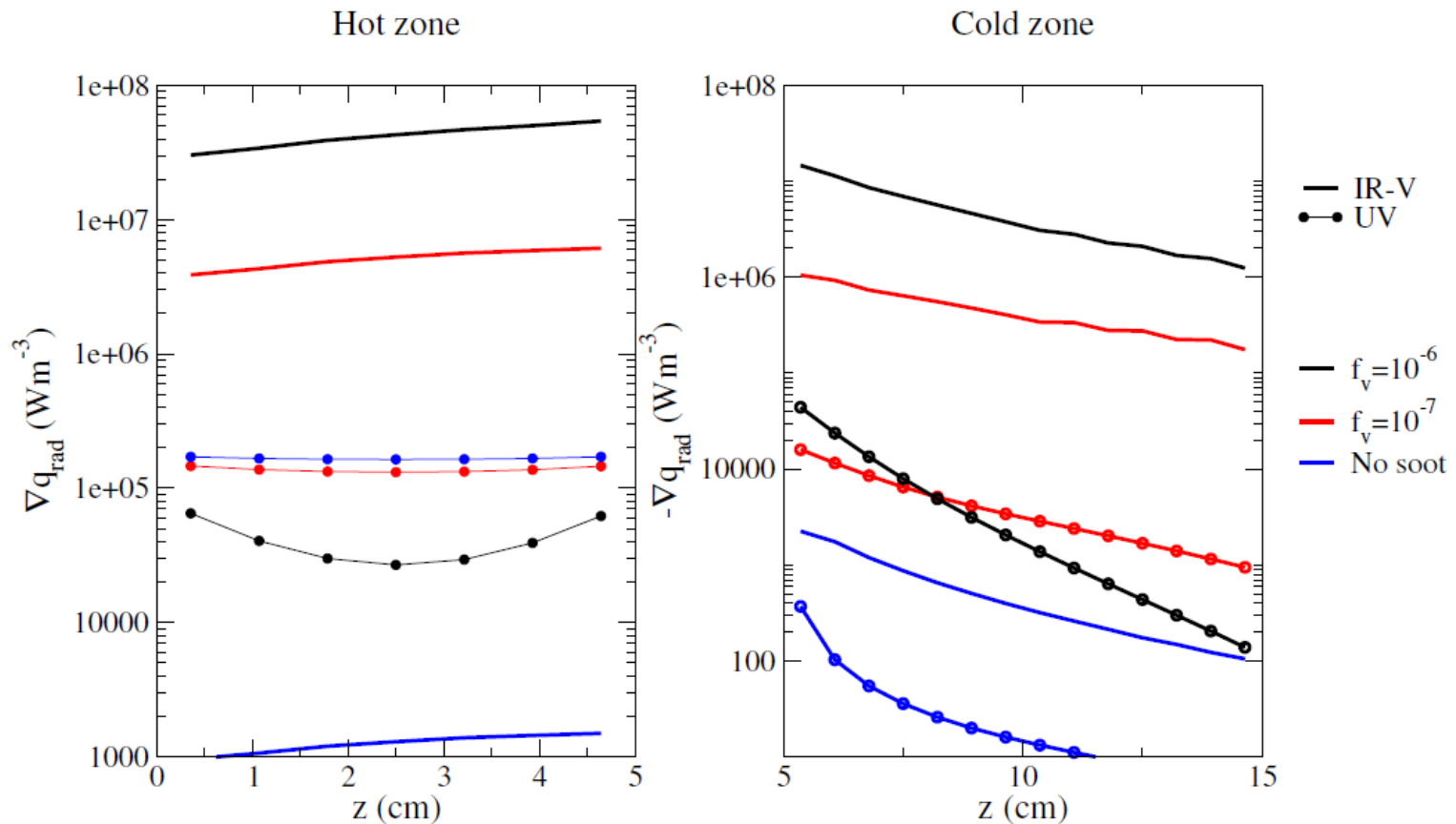


Figure 8. Radiative power distribution along the axis of the reactor with uniform soot distribution. Full lines correspond to IR region and Dashed lines with circles correspond to UV region. The colors indicate the soot volume fraction. Calculations are carried out with 20×20 spatial mesh and $N_\theta = N_\phi = 40$.